Cellular and Molecular Life Sciences (2019) 76:3621–3640
https://doi.org/10.1007/s00018-019-03088-3

Cellular and Molecular Life Sciences

ORIGINAL ARTICLE

ATAT1 regulates forebrain development and stress-induced tubulin hyperacetylation

Lin Li[1,2] · Sriram Jayabal[3] · Mohammad Ghorbani[1,2] · Lisa-Marie Legault[4] · Serge McGraw[4] · Alanna J. Watt[3] · Xiang-Jiao Yang[1,2,5,6]

Received: 2 November 2018 / Revised: 18 March 2019 / Accepted: 27 March 2019 / Published online: 5 April 2019
© Springer Nature Switzerland AG 2019

Abstract

α-Tubulin acetyltransferase 1 (ATAT1) catalyzes acetylation of α-tubulin at lysine 40 in various organisms ranging from *Tetrahymena* to humans. Despite the importance in mammals suggested by studies of cultured cells, the mouse *Atat1* gene is non-essential for survival, raising an intriguing question about its real functions in vivo. To address this question, we systematically analyzed a mouse strain lacking the gene. The analyses revealed that starting at postnatal day 5, the mutant mice display enlarged lateral ventricles in the forebrain, resembling ventricular dilation in human patients with ventriculomegaly. In the mice, ventricular dilation is due to hypoplasia in the septum and striatum. Behavioral tests of the mice uncovered deficits in motor coordination. Birth-dating experiments revealed that neuronal migration to the mutant septum and striatum is impaired during brain development. In the mutant embryonic fibroblasts, we found mild defects in cell proliferation and primary cilium formation. Notably, in these cells, ATAT1 is indispensable for tubulin hyperacetylation in response to high salt, high glucose, and hydrogen peroxide-induced oxidative stress. We investigated the role of ATAT1 in the hematopoietic system using multicolor flow cytometry and found that this system remains normal in the mutant mice. Although tubulin acetylation was undetectable in a majority of mutant tissues, residual levels were detected in the heart, skeletal muscle, trachea, oviduct, thymus and spleen. This study thus not only establishes the importance of ATAT1 in regulating mouse forebrain development and governing tubulin hyperacetylation during stress responses, but also suggests the existence of an additional α-tubulin acetyltransferase.

Keywords Lateral ventricle · Ventricular dilation · Septum · Striatum · Stress signaling

Introduction

Acetylation of α-tubulin was first identified in the early 1980s with the flagella of the single-cell green alga *Chlamydomonas reinhardtii* [1]. Amino acid sequencing subsequently identified lysine 40 as the acetylation site [2]. This site is conserved from protists to mammals [3, 4] and is also present in flowering plants [5], but not in yeast [6]. A monoclonal antibody specific for the acetylated form was then developed and found to recognize α-tubulin from various organisms [4]. Commercially available for over two decades, this antibody (known as clone 6-11B-1) has been widely used as a marker of stable microtubules. Tubulin acetylation is a marker for long-lived stable microtubules and abundant in axons and structures such as flagella and cilia. Numerous studies have been carried out using cells cultured in vitro and from these studies it was concluded that acetylation of α-tubulin is important for various cellular and perhaps also

✉ Xiang-Jiao Yang
xiang-jiao.yang@mcgill.ca

1 The Rosalind and Morris Goodman Cancer Research Center, McGill University, 1160 Pine Avenue West, Montreal, QC H3A 1A3, Canada

2 Department of Medicine, McGill University, Montreal, Canada

3 Department of Biology, McGill University, Montreal, Canada

4 Department of Obstetrics and Gynecology, Faculty of Medicine, Université de Montréal, Montreal, QC, Canada

5 Department of Biochemistry, McGill University, Montreal, Canada

6 McGill University Health Center, Montreal, QC, Canada

developmental processes. For example, tubulin acetylation was proposed to play roles in regulating microtubule architecture [7, 8] and intracellular transport [9, 10]. Such conclusions were challenged about a decade ago, when the responsible deacetylase HDAC6 [11–13] was genetically inactivated in mice and no major phenotypes were observed [14]. The important issue about whether this modification is a cause or consequence in different biological processes remains an interesting question awaiting further investigation [15].

As for the responsible acetyltransferase, worm Mec-17 was first identified as the α-tubulin acetyltransferase [16, 17]. The importance of tubulin acetylation in vertebrates was implied in the study showing that knockdown of *mec-17* expression by morpholinos led to zebrafish developmental defects, including curved body shape, short body axis, hydrocephalus, small heads, small eyes and neuromuscular dysfunction [16]. Two other studies either using shRNA to knockdown *Atat1* (paralogous to Mec-17) or deleting *Elp3* in the mice showed that loss of tubulin acetylation affected neuronal migration and differentiation in the mouse cerebral cortex [18–20]. These studies suggested a major role for tubulin acetylation in mammalian development. While germline deletion of *Atat1* led to complete tubulin acetylation loss in many tissues and confirmed ATAT1 as the bona fide α-tubulin acetyltransferase in mice [21, 22], the mice are viable and fertile, displaying a mild distortion in the dentate gyrus, an impairment of sperm motility and slightly reduced litter size [21, 22]. While contradicting the important roles of tubulin acetylation suggested by various studies with cultured cells in vitro, these results from the mouse genetic studies are consistent with the earlier knockout report on HDAC6 [14].

Because ATAT1 is evolutionarily conserved from *Tetrahymena* to humans [16, 17], it must be critical for some biological processes, raising the important question what roles this enzyme really has in mammals. A recent report indicated that ATAT1 is required for touch sensation in mice [23], but the question about the roles in vivo needs to be investigated further. A very preliminary observation in our previous study of the *Atat1*$^{-/-}$ mice is that their lateral ventricles are large [21]. This abnormality is peculiar and has not been substantiated [21], so we followed this initial lead to determine the function of ATAT1 in vivo. Now, we have systematically analyzed serial sections from the mutant brain. The analyses have confirmed the ventricular dilation and further revealed that it starts at postnatal day 5 due to hypoplasia in the septum and striatum. We discovered that the anomaly is due to defective neuronal migration. Related to the striatal defects, behavioral tests identified defective motor coordination.

In mouse embryonic fibroblasts (MEFs), we found that loss of *Atat1* has minor effects on proliferation and primary cilia formation. As recently reported [24], we confirmed that stress conditions, such as exposure to high salt, high glucose and oxidative stress, induce acute tubulin hyperacetylation. Importantly, the stimuli failed to induce any tubulin acetylation in mutant MEFs, indicating that stress-induced tubulin hyperacetylation is solely dependent on ATAT1. The role of *Atat1* in the blood system remains unclear, so we have also analyzed different hematopoietic cells. Flow cytometry revealed that composition of these cells is similar in wild-type and *Atat1*$^{-/-}$ bone marrows, indicating that ATAT1 is dispensable for hematopoiesis. While this is the major bone fide α-tubulin acetyltransferase in many tissues [21, 22], we also observed residual tubulin acetylation in the mutant heart, skeletal muscle, trachea, oviduct, thymus and spleen, thereby suggestive of another α-tubulin acetyltransferase in these tissues. Thus, this study highlights defective forebrain development and complete loss of stress-induced tubulin hyperacetylation as major phenotypes in the mutant mice.

Results

Atat1 inactivation causes ventricular dilation in the mouse forebrain

Atat1$^{-/-}$ mice are born normally and also fertile, with no obvious defects in appearance [21, 22]. From the previous brain sections, we noticed that the lateral ventricles are larger in the mutant forebrain [21]. To verify and extend this preliminary observation, we carried Nissl staining of serial brain sections from wild-type and *Atat1*$^{-/-}$ mice. For this, we systematically compared sagittal sections from three pairs of wild-type and mutant brain at 24 days and 8 months after birth. Shown in Fig. 1a, b are two pairs of representative sagittal sections. At both time points, we observed significantly larger lateral ventricles in the mutant forebrain. Consistent with this, the transverse and coronal brain sections also displayed a larger lateral ventricle in the *Atat1*$^{-/-}$ mice at 2 and 12 months (Fig. 2a, b and data not shown). Of note, this dilation is the most prominent in the middle part of serial sections. The dilation of lateral ventricles observed in the mutant mice differs from the dilation in typical hydrocephalus. While a bulge is frequently observed on the head of mice with hydrocephalus symptoms [25], no such bulges were observed in 12-month-old or younger *Atat1*$^{-/-}$ mice (Fig. 1c and data not shown). To trace the developmental origin of the defect, we investigated when dilation of the lateral ventricle becomes obvious during brain development prior to or after birth. For this, we carried out Nissl staining using serial transverse sections from wild-type and mutant brains at E17.5, P1, P5 and P15. Larger lateral ventricles were observed as early as P5 (Fig. 2c–f). This dilation did not appear to affect overall health and life

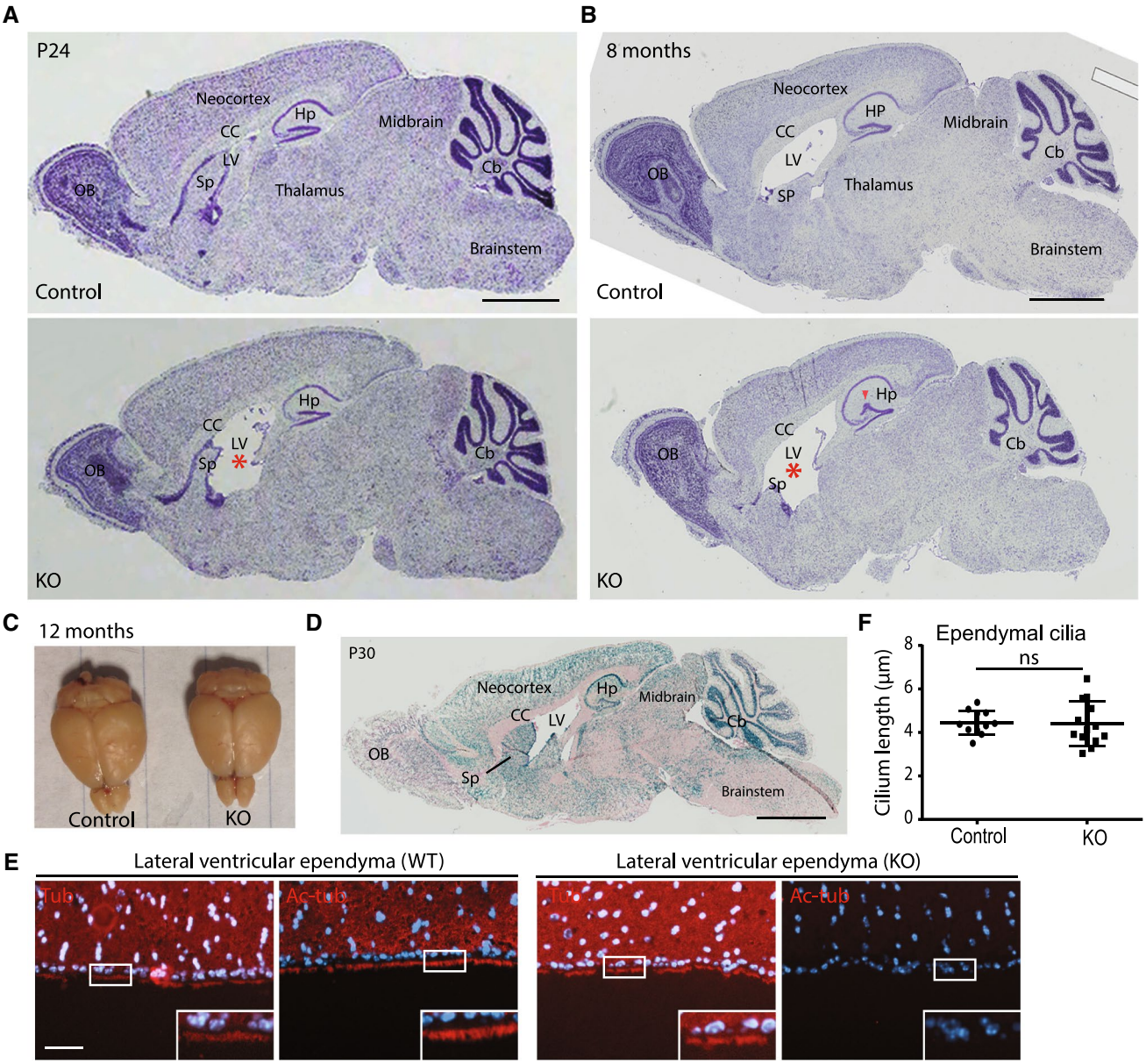

Fig. 1 Mouse *Atat1* loss causes ventricular dilation in the forebrain. **a**, **b** Nissl staining of sagittal brain sections prepared from 24-day- or 8-month-old mice. Lateral ventricles are much more expanded in the *Atat1*$^{-/-}$ knockout (KO) mouse brain (marked with red asterisks in the mutant sections). Note prominent hypoplasia in the septum. A red arrowhead in the mutant section at the right denotes distortion of the dentate gyrus, as reported previously [21]. Other structures, such as the neocortex, corpus callosum, cerebellum, thalamus, mid-brain and olfactory bulb, are similar in wild-type and *Atat1*$^{-/-}$ mice. Scale bar, 1 mm. **c** Representative top view images of the whole brains from 12-month-old wild-type and *Atat1*$^{-/-}$ mice. **d** β-Gal staining of a sagittal brain section from a P30 *Atat1*$^{-/-}$ mouse. Scale bar, 1 mm. These particular mice still contained a promoter-less LacZ cassette inserted at the *Atat1* locus [21]. **e** Immunofluorescene microscopic images of lateral ventricular ependyma. Anti-tubulin (Tub) and -acetyl-tubulin (Ac-Tub) antibodies were used and merged images with DAPI staining are shown here. Images for ependymal cilia were enlarged and shown in the right bottom. Scale bar, 30 µm. **F**, length of ependymal cilia in lateral ventricles (as in panel E; multiple positions were measured from 2 pairs of mice). *ns* not statistically significant. *Cb* cerebellum, *CC* corpus callosum, *Hp* hippocampus, *LV* lateral ventricle, *OB* olfactory bulb, *Sp* septum

span of *Atat1*$^{-/-}$ mice, because no overall differences were observed regarding body weight and general health condition for wild-type and mutant littermates for up to 24 months of age. Thus, *Atat1* deletion causes ventricular dilation in the forebrain as early as P5.

Atat1 loss causes hypoplasia in the septum and striatum of the forebrain

From the stained transverse brain sections, we observed a thinner septum (Fig. 2a, lower panel) and a smaller

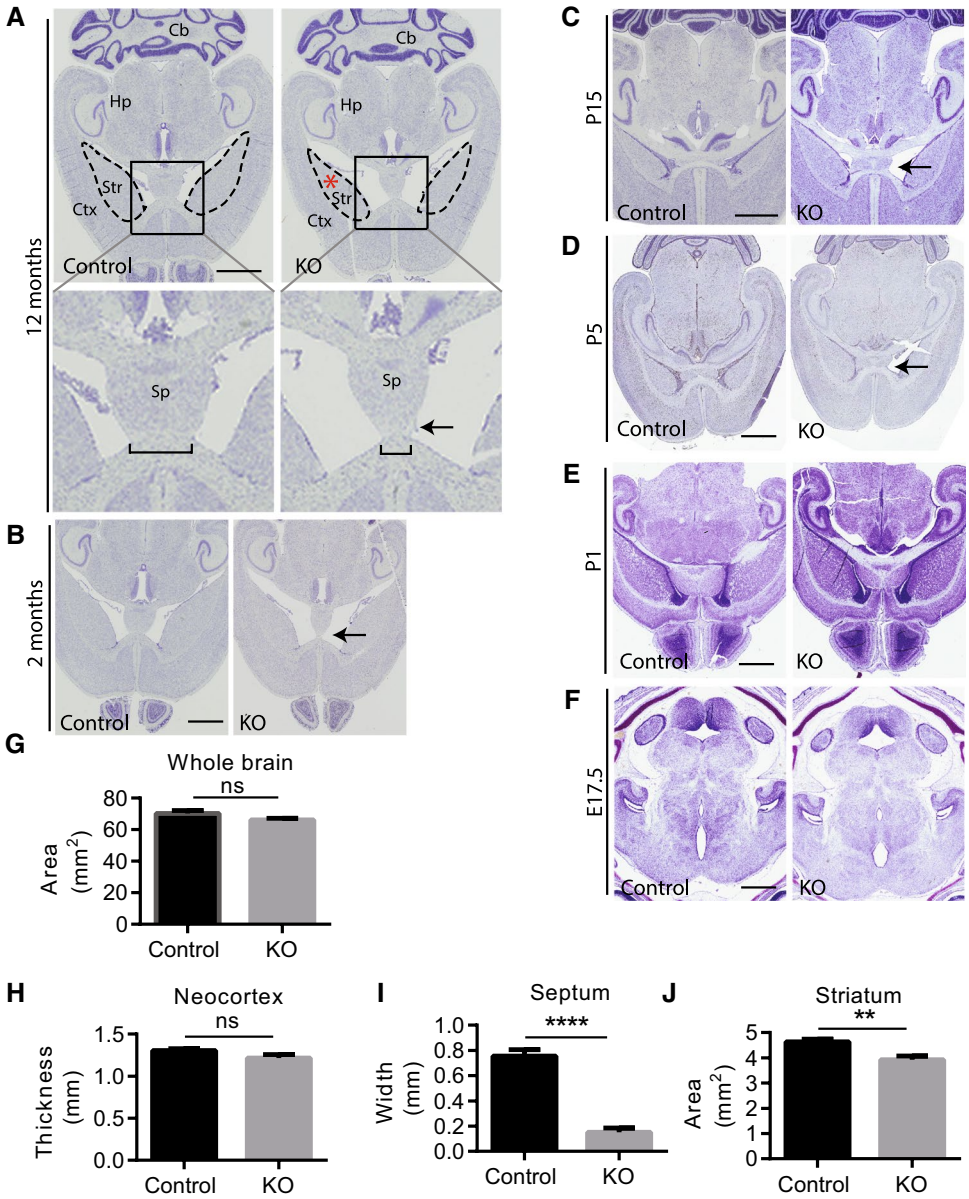

Fig. 2 Ventricular dilation in the mutant brain due to septal and striatal hypoplasia. **a**–**f** Nissl staining for transverse brain sections from adult mice at 12 and 2 months of age (**a**, **b**); pups at P1, P5 and P15 (**c**–**e**); or embryos at E17.5 (**f**). Arrows in **a**–**d** denote that the bottom part of the mutant septum is thinner than in the wild type. The mutant lateral ventricles are larger than the wild-type counterparts. The mutant sections at P5 and P15 were tilted, but at these developmental stages there is no empty space visible in wild-type lateral ventricles. The boundary of the striatum is demarcated with dashed lines. The red asterisk in the top left panel in **A** marks the small mutant striatum. The wild-type and mutant brains were serially sectioned; the sections from similar position were used for Nissl staining. Scale bars, 2 mm (**a**, **b**), 1 mm (**c**, **d**), 500 µm (**e**, **f**). *Cb* cerebellum, *Hp* hippocampus, *Sp* septum, *Str* striatum. **g** Area of whole brain measured from transverse brain sections (3 pairs of mice, 2 sections from each mouse). *ns* not statistically significant. **h** Thickness of the neocortex in the middle part was measured from transverse brain sections (3 pairs of mice, 2 sections each mouse). **i** Width of the septum measured at the bottom part of septum (3 pairs of mice, 2 sections for each mouse). Paraffin-embedded brains were serially sectioned to obtain paired transverse sections, with sections showing the most obvious ventricular dilation used for measurement. **j** Area of the striatum measured from transverse brain sections (3 pairs of mice, 2 sections for each mouse). For **g**–**j** data are represented as mean ± sem; *ns* not statistically significant; $^{**}p<0.01$; $^{****}p<0.0001$

striatum (Fig. 2a, indicated by a red asterisk) in the *Atat1*$^{-/-}$ brain, while the other brain structures such as the cerebral cortex and cerebellum appear normal (Fig. 2a). To confirm this quantitatively, we measured the size of the whole brain, thickness of the neocortex, size of the striatum, and width at the bottom part of the septum using

paired wild-type and *Atat1*$^{-/-}$ transverse brain sections. In serial stained sections, those that displayed the most obvious lateral ventricle dilation were used for measurement. While thickness of the overall brain and neocortex are comparable between the wild-type and mutant mice (Fig. 2g, h), the mutant septum is much thinner (Fig. 2i). Albeit less dramatic, the mutant striatum is significantly smaller than that of the wild type (Fig. 2j).

Ependymal cilia in the brain ventricles are important for the circulation of cerebrospinal fluid. Dysfunction of ependymal cilia in the ventricles causes a blockade in the cerebrospinal fluid circulation and leads to larger ventricular dilation in the brain [26]. Tubulin acetylation is abundant in the cilia and might have roles in cilia functioning [27]. A knockin *LacZ* reporter is harbored within the mutant allele of the heterozygous *Atat1*$^{+/-}$ mice [21], so we used the reporter to detect *Atat1* expression by β-galactosidase staining. We found that *Atat1* is highly expressed throughout the brain, not only in the ependymal cells of the lateral ventricle, where ependymal cilia reside, but also in the septum, striatum, and cerebral cortex (Fig. 1d). We showed that tubulin acetylation was detectable in the wild-type, but not mutant ependymal cilia (Fig. 1e). However, the length of ependymal cilia is comparable between wild-type and mutant mice (Fig. 1f), indicating that a loss of *Atat1* and tubulin acetylation does not affect ependymal cilia assembly in lateral ventricles. Thus, loss of *Atat1* and tubulin acetylation leads to larger lateral ventricles mainly due to hypoplasia in the septum and striatum.

Atat1 loss does not affect mouse neocortical development

It was reported that shRNA knockdown of mouse *Atat1* [18] or inactivating *Elp3* [28] causes neuronal migration and differentiation defects in the cerebral cortex. Nissl staining revealed that thickness of the cerebral cortex was not affected in the mutant brain (Fig. 2h). To further investigate whether loss of *Atat1* affects neocortical development, we performed indirect immunofluorescence microscopy using antibodies against the neural stem and progenitor cell (NSPC) markers such as Sox2 and Tbr2. As shown in Fig. 3a–d, NSPC development is not affected in the mutant neocortex. We also tested antibodies specific to the cortical lamination markers such as Cux1, Cux2, Tbr1 and Ctip2. As shown in Fig. 3e, f, similar patterns of these lamination markers were observed in the wild-type and mutant neocortices, indicating that neocortical lamination is not affected in the mutant. Golgi staining revealed no obvious abnormalities in the neural trees and dendrites (Fig. 3g, h). Thus, loss of *Atat1* does not affect neocortical development.

Effects of *Atat1* loss on neuronal migration during septal and striatal development

Neurogenesis is dynamic during gestation. To trace how neurons are produced and then migrate in the brain, we injected bromodeoxyuridine (BrdU) intraperitoneally into pregnant mice at E13.5 and recovered the brain at day 10 after pups were born. This time point was chosen because ventricular dilation is already obvious in the mutant brain (Fig. 2a–f). After immunohistochemical staining with anti-BrdU monoclonal antibody, we counted positively stained cells in the striatum, septum and neocortex. For the latter, we divided the neocortical layer from the subventricular zone to the molecular zone equally into ten sub-layers (Fig. 4d) to count BrdU^{+} cells in each sub-layer. When counting positively stained cells in the striatum, septum and neocortex, we considered those with darkly stained nuclei as dense labels and those with lightly stained nuclei as light labels. We found that compared to the wild-type counterpart, there were significantly fewer BrdU^{+} cells (both densely and lightly labeled) in the mutant striatum (Fig. 4a, b) and septum (Fig. 4a, c), suggesting that neuronal migration to these regions are impaired. By contrast, no major difference was observed between the wild-type and mutant neocortices (Fig. 4d–f); consistent with this, no neocortical lamination defects were present in the mutant brain (Fig. 3e, f).

To investigate whether loss of *Atat1* affects NSPC proliferation, we injected BrdU intraperitoneally into P10 pups. After 1 h, their brain was recovered for immunohistochemical staining against anti-BrdU monoclonal antibody and counting BrdU^{+} cells close to the subventricular zone. As shown in Fig. 4g, h, the number of BrdU^{+} NSPCs was comparable between the wild-type and *Atat1*$^{-/-}$ subventricular zones, indicating that loss of *Atat1* does not affect the S-phase of NSPCs. To substantiate this, we stained E14.5 embryonic and P0 brain sections using an anti-Ki67 antibody. As shown in Fig. 4i, there were no differences between the wild-type and *Atat1*$^{-/-}$ mice, supporting NSPC proliferation is not affected. *Atat1* loss was reported to promote apoptosis in seminiferous tubules [22]. To test whether apoptosis is affected in the mutant brain, we carried out TUNEL staining using brain sections from wild-type and *Atat1*$^{-/-}$ mice. No significant difference was observed regarding the number of TUNEL^{+} cells in the striatum between the wild-type and mutant groups at both E14.5 and P24 (Fig. 4j). These results support that loss of *Atat1* causes defective cell migration to the striatum and septum, but does not affect other NSPC properties.

Mouse *Atat1* loss leads to motor coordination deficits

To determine the possible functional impact of striatal and septal hypoplasia, we carried out a battery of behavioral

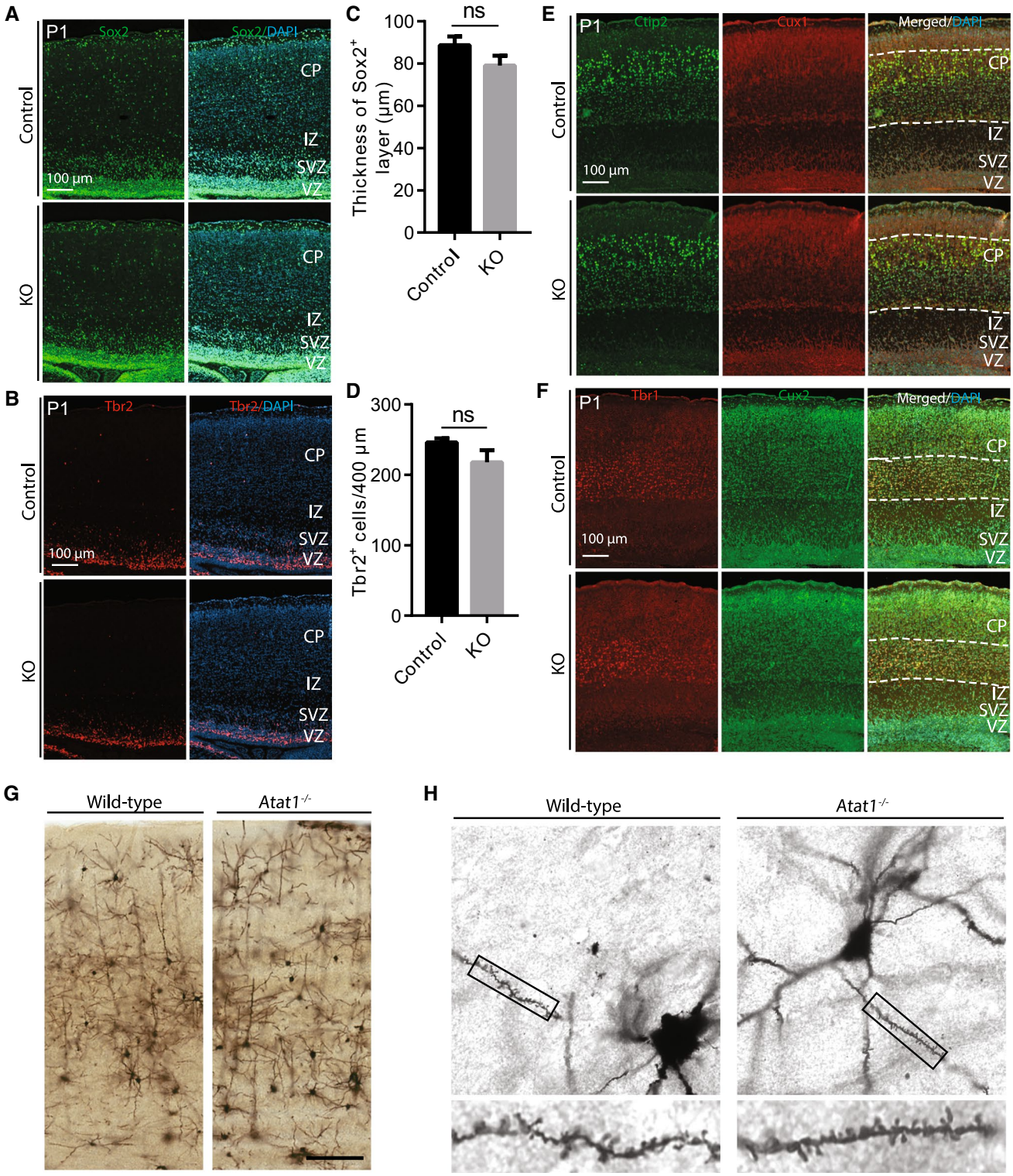

tests. The open field test revealed no overall difference between control and *Atat1*$^{-/-}$ mice (Fig. 5a–c). The time the mice spent in the center area (Fig. 5a) and total distance traveled (Fig. 5b) in the arena were comparable between the wild-type and mutant groups. The feces were counted during the open field tests as indicators for the anxious status of mice. We counted the feces, but found no significant difference between the wild-type and mutant groups (Fig. 5c). The tail suspension test revealed no statically significant difference regarding the immobile time (which is an indicator

◂**Fig. 3** Grossly normal development of the cerebral cortex in *Atat1*-null mice. **a**, **b** Immunofluorescence microscopy to detect $Sox2^+$ neural stem cells (NSCs) and $Tbr2^+$ neural progenitor cells (NPCs) on P1 brain sections. The thickness of $Sox2^+$ layer was measured and shown in **c** (2 pairs of mice, with 2 sections from each mouse), the number of $Tbr2^+$ cells was counted and is shown in **d** (2 pairs of mice, with 2 sections from each mouse). Data are represented as mean ± sem; ns, not statistically significant. **c**, **d** Statistical analysis of the results from **a** and **b**, respectively. **e** Immunofluorescence microscopic detection of $Cux1^+$ and $Ctip2^+$ neurons. Dashed lines demarcate $Ctip2^+$ layers. **f** Immunofluorescence detection of $Tbr1^+$ and $Cux2^+$ neurons. A white dotted line indicates the $Tbr1^+$ layer. **g** Images of wild-type and knockout neocortices from Golgi-stained brain sections. Note that there is no difference between the wild-type and mutant sections in many other slides not shown here. **h** High-magnification images of dendritic spines. *CP* cortical plate, *IZ* intermediate zone, *SVZ* subventricular zone, *VZ* ventricular zone

for depression) between the wild-type and $Atat1^{-/-}$ groups (Fig. 5d). Accelerated rotarod tests were utilized to check the motor coordination ability of the mice [29]. For these tests, each mouse was subjected to four tests per day (with a break of at least 20 min between 2 tests) for four consecutive days. The latent time for each test in a single day (Fig. 5e–g) and the average latent time for each mouse in 4 days were recorded (Fig. 5h). As shown by a shorter average latent time (Fig. 5e–g), $Atat1^{-/-}$ mice were prone to fall. This trend was the most obvious in 6 months old mice (Fig. 5f). Thus, loss of *Atat1* results in mild defects in motor coordination.

Atat1 deletion exerts minor effects on MEF proliferation and cilia formation

We next investigated how *Atat1* loss might affect the characteristics of MEFs. In $Atat1^{-/-}$ MEFs, while the overall microtubule network is normal as shown by immunofluorescence using anti-tubulin antibody (Fig. 6a, left panel), tubulin acetylation is completely lost as shown by immunofluorescence staining against anti-acetyl-tubulin monoclonal antibody (Fig. 6a, right panel). 20,000 MEF cells were seeded per well in 12-well plates and the growth rate was measured by the IncuCyte Imaging System. *Atat1*-null MEFs grew slightly faster than the wild type in the first few days, but showed no difference from wild-type MEFs afterward (Fig. 6b).

Primary cilium is important in cell signaling and tubulin acetylation is enriched in this organelle [30]. By immunostaining of type III adenylyl cyclase (ACIII) as a marker for primary cilia, we found that tubulin acetylation is totally lost in the mutant primary cilia (Fig. 6c). Serum starvation or growth to confluency induces primary cilia formation, whereas heat shock for a short time induces primary cilia resorption [31]. To study how tubulin acetylation affects primary cilia formation, we grew MEFs to confluency and treated them with either EBSS media (for serum starvation) for 4 h or incubation at 42 °C for 30 min. In the no treatment group, there were comparable numbers of wild-type and mutant MEFs possessing primary cilia (WT 38% vs KO 45%, $p = 0.29$). Similarly, after serum starvation or heat shock, the number of MEFs possessing primary cilia was also comparable between of the wild-type and mutant (WT 58% vs KO 59% for EBSS starvation, $p = 0.79$; WT 50% vs KO 42% for heat shock, $p = 0.16$). We also measured the ciliary length. As shown in Fig. 6d, the primary cilia length was also comparable in the wild-type and mutant MEFs. However, after serum starvation or heat shock, the mutant primary cilia were significantly longer even though the difference was small (Fig. 6d), indicating that ATAT1 is required for optimal primary cilia formation. In comparison, the length of ependymal cilia in the lateral ventricle was comparable in wild-type and $Atat1^{-/-}$ mice (Fig. 1f). Thus, *Atat1* loss only exerts minor effects on primary cilia formation. It was reported that tubulin acetylation regulates autophagy [32, 33]. To verify this, Western blotting was carried out using MEF extracts against anti-LC3 antibody. There was no difference of the LC3b-II/LC3b-I ratio between the wild-type and mutant MEFs (Fig. 6e, f), indicating that autophagy is not affected in the mutant. Therefore, *Atat1* loss exerts mild effects on MEF proliferation and primary cilia formation.

Atat1 is essential for stress-induced tubulin hyperacetylation

A recent study demonstrated that cellular stress stimuli, such as exposure to H_2O_2 or high concentration of NaCl, induce tubulin hyperacetylation [24]. As shown in Fig. 7a, upon treatment with 0.25 M NaCl, 5 mM H_2O_2 or 100 mM glucose for 30–60 min, tubulin acetylation increased by 2.8- to 11-fold in wild-type MEFs (Fig. 7a, compare lanes 1, 3, 5 and 7). In stark contrast, there was no tubulin acetylation detected in $Atat1^{-/-}$ MEFs, with or without treatments (lanes 2, 4, 6 and 8). Indirect immunofluorescence microscopy with anti-acetyl-tubulin antibody confirmed that treatment with 125 or 250 mM NaCl induced tubulin hyperacetylation in the wild-type, but not mutant MEFs (Fig. 7b). There was no overall morphological difference between the wild-type and $Atat1^{-/-}$ MEFs (Fig. 7b, left two panels). As with NaCl treatment, serum starvation in the EBSS media induced tubulin hyperacetylation in the wild-type, but not mutant MEFs (Fig. 7b). Thus, tubulin hyperacetylation is induced in wild-type MEFs in response to cellular stresses, but such responses are lost completely in $Atat1^{-/-}$ MEFs.

Grossly normal hematopoiesis and residual tubulin acetylation in $Atat1^{-/-}$ mice

Because it remains unclear about the role of *Atat1* in the blood system, we analyzed hematopoietic cells

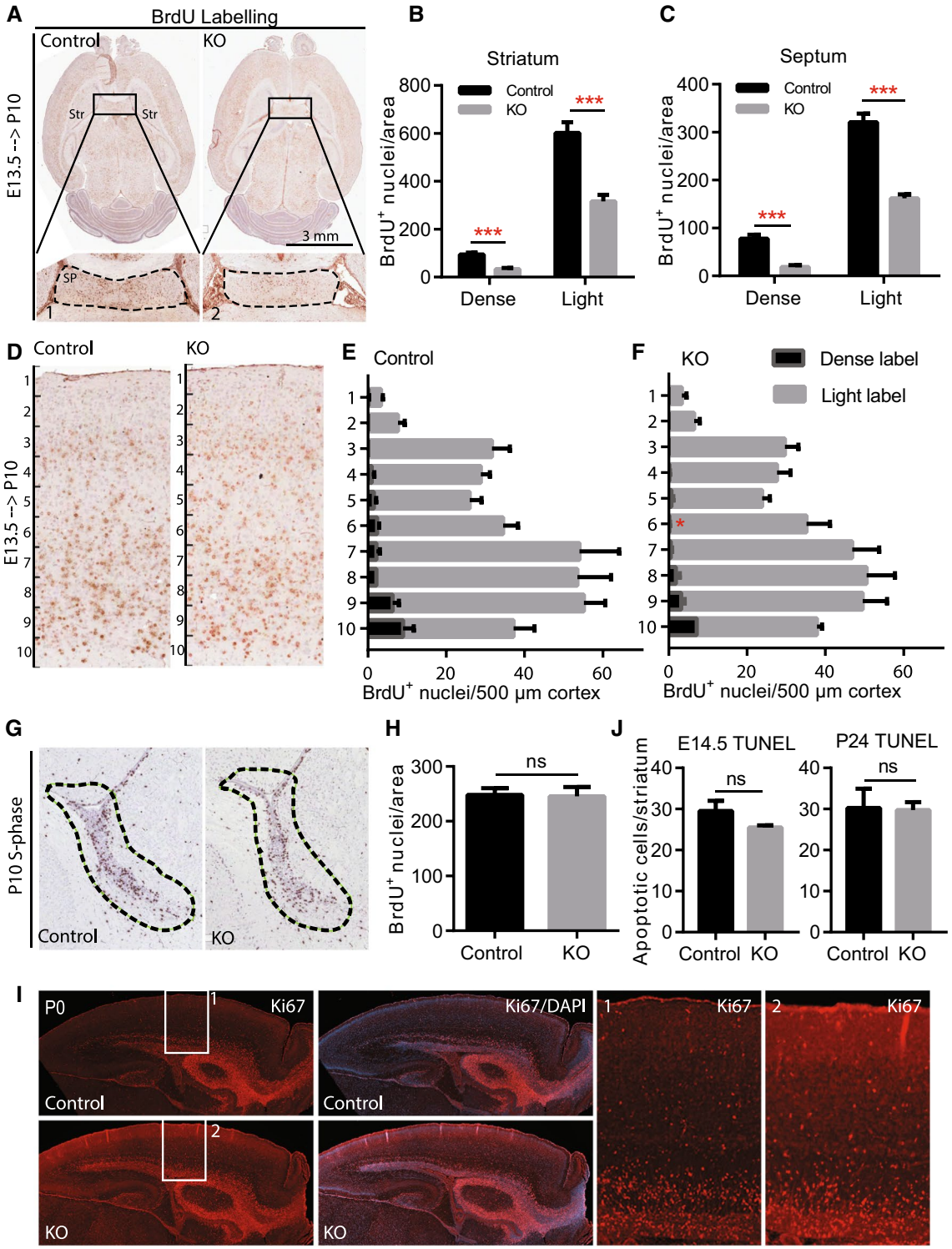

systematically. As shown in Table 1, complete blood counts revealed that various blood cells were not affected (Table 1). In addition, biochemical analyses revealed no difference between the wild-type and mutant blood (Table 2). To explore how hematopoiesis is affected upon *Atat1* deletion, we carried out systematic flow cytometric analyses of cells in the bone marrow compartment. As shown in Fig. 8a–g, hematopoietic stem cells, progenitors and other cells were not affected in the mutant bone marrow compartment. In light of residual levels of histone acetylation in the thymus, spleen and other tissues, we investigated whether tubulin acetylation is affected in the mutant bone marrow. We found

◂**Fig. 4** BrdU tracing of neuronal migration in wild-type and *Atat1*$^{-/-}$ brains. **a** BrdU was injected into E13.5 pregnant mice intraperitoneally, and the brains were collected from pups at P10. The boxed septal areas in the upper panels were enlarged and shown in the lower panels. *Str* striatum, *SP* septum. **b**, **c** Quantification of BrdU^{+} densely or lightly labeled cells in the striatum and septum ($n=3$, with 2 sections for each mouse). ***$p<0.001$. The boundary of the septum was demarcated with dashed lines. If the nucleus was fully dark, it was counted as being densely labeled; otherwise the cell was considered to be lightly labeled. **d–f** Cerebral cortex above the hippocampus was equally divided into ten zones. BrdU^{+} cells in each zone were counted and shown in panels **e** (control) and **f** (KO) ($n=3$, with 2 sections for each mouse). **g**, **h** 1-h BrdU incorporation into neural stem and progenitor cells in wild-type and *Atat1*$^{-/-}$ mice. One hour after BrdU injection, P10 pups were killed for immunohistochemical analysis using anti-BrdU monoclonal antibody. Representative images are shown in **g**. The incorporated BrdU^{+} cells near the lateral ventricle area (demarcated with dashed dark curves) were counted and shown in **h** ($n=3$, with 2 sections for each mouse). **i** Representative images showing that Ki67^{+} signals are comparable between control and mutant neonatal brain sections. The neocortices were enlarged and are shown in the right two panels. All quantitative data are represented as mean ± sem; *ns* not statistically significant

that tubulin acetylation is totally lost in the *Atat1*$^{-/-}$ bone marrows. Taken together, these results indicate that hematopoiesis is not affected in the mutant mice.

While ATAT1 is the sole tubulin acetyltransferase in the brain and many other tissues [21, 22], we observed residual signals of tubulin acetylation in the mutant trachea and oviduct by immunofluorescence microscopy (Fig. 9a, b). By contrast, the acetylation was completely absent in the mutant lateral ventricles (Fig. 1e), MEFs (Fig. 7a) and olfactory ependyma (Fig. 9c). Moreover, immunoblotting confirmed the residual levels of tubulin acetylation in the mutant trachea and oviduct (Fig. 9e, f). Moreover, such residual levels were also detected in the mutant heart, thymus, spleen and skeletal muscle (Fig. 9e, f). These results strongly suggest the existence of a minor tubulin acetyltransferase in the tissues where residual tubulin acetylation is still detectable upon *Atat1* deletion.

Discussion

This study substantiates the previous preliminary finding that *Atat1*$^{-/-}$ mice show enlarged lateral ventricles in the brain [21]. We have now confirmed the ventricular dilation in the adult mutant brain and discovered that the dilation starts at P5 (Figs. 1, 2). We demonstrated that the dilation is due to septal and striatal hypoplasia in the forebrain (Figs. 1, 2) and identified defective neuronal migration as one underlying cause (Fig. 4). The role of *Atat1* in the blood system remains elusive, so we have also analyzed hematopoietic cells systematically. We observed similar cellular composition in the wild-type and *Atat1*$^{-/-}$ bone marrows (Fig. 8), indicating ATAT1 is not essential for hematopoiesis in that compartment. In the MEFs, we found loss of *Atat1* has minor effects on proliferation and primary cilia formation (Fig. 6). As reported [24], stress conditions, such as exposure to high salt, high glucose and H_2O_2-induced oxidative stress, induces tubulin hyperacetylation in cultured MEFs (Fig. 7). Intriguingly, these stimuli failed to induce any tubulin acetylation in *Atat1*$^{-/-}$ MEFs, indicating that tubulin hyperacetylation in response to cellular stress stimuli acts through ATAT1 (Fig. 7). This is important as stress responses are critical for organism survival under adverse conditions. While ATAT1 is the major bone fide tubulin acetyltransferase [21, 22], there are residual signals of tubulin acetylation in the mutant trachea, oviduct, heart, thymus, spleen and skeletal muscle, which, for the first time, suggests the existence of another tubulin acetyltransferase that is responsible for residual tubulin acetylation in these tissues.

Tubulin acetylation was previously reported to play a role in neuronal migration and differentiation in the cerebral cortex [18, 28]. Our results using *Atat1*$^{-/-}$ mice show that although tubulin acetylation is totally depleted, cerebral cortical development is not affected (Figs. 2h, 3). One previous study utilized shRNA to knockdown *Atat1* and might produce off-target effects [18]. Another study reported neuronal migration and differentiation defects [28], perhaps due to loss of *Elp3* itself rather than defective tubulin acetylation. Although we did not detect abnormality in the cerebral cortex, we observed smaller striatum and thinner septum in the *Atat1*$^{-/-}$ brain (Figs. 1, 2). The striatum is a critical component of the motor and reward system in mice. It receives glutamatergic and dopaminergic inputs from the motor cortex and sends outputs to the rest parts of the basal ganglia [34]. Using accelerated rotarod tests, we found that mice lacking *Atat1* have mild defects in motor coordination (Fig. 5e–h). The defective motor coordination might be due to the hypoplasia in the striatum and septum of the *Atat1*-deficient mice, but we cannot exclude other possibilities. For example, muscle function might also be affected. The open field test showed that the mutant mice travelled similar as the wild-type (Fig. 5b), indicating it is not so likely that muscle function is compromised. The striatum and septum are also involved in regulating anxiety behaviors, but we observed no difference in the open field and tail suspension tests (Fig. 5a–d).

Striatal abnormalities are of clinical significance to various movement disorders. For example, Parkinson's disease is mainly due to loss of dopaminergic innervation to the dorsal striatum. Striatal atrophy is also important for Huntington's disease and other movement disorders such as chorea and dyskinesia. The motor coordination defects observed in the mutant mice somewhat resemble those in Huntington's disease, an inherited neurodegenerative disorder characterized by massive loss of medium spiny neurons, which constitute 95% cells in the striatum [35]. The disease shows a

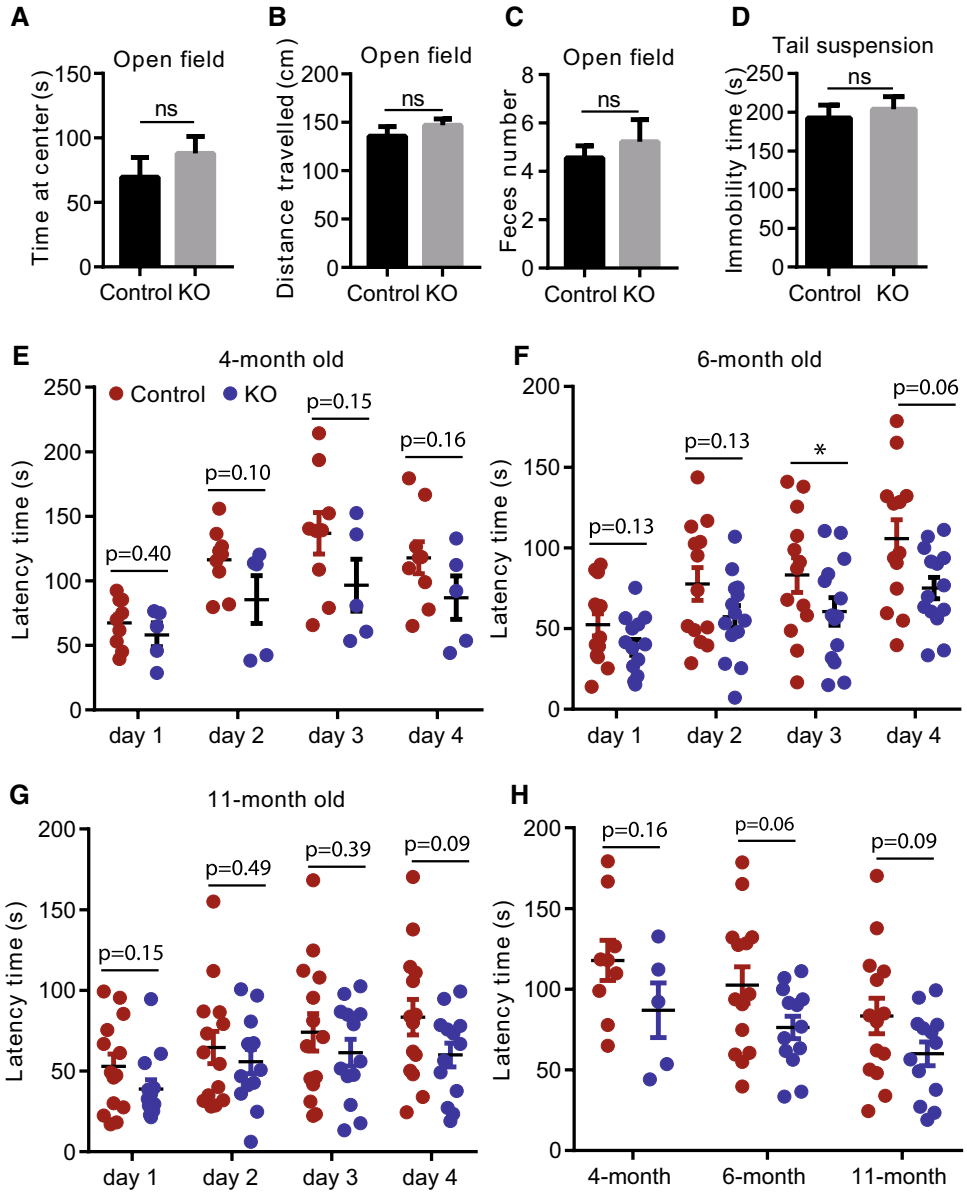

Fig. 5 Behavioral tests of the wild-type and *Atat1*$^{-/-}$ mice. **a–c** Open field tests were carried out in a 40 × 40 × 40 cm arena ($n=9$ for the control or *Atat1*$^{-/-}$ mice). The time that the mice spent at the center of the arena (20 × 20 cm; each mouse was tested for 10 min) is shown in **a**, whereas the distance that they travelled in the arena is presented in **b**. Feces per mouse in the open field tests were counted and the number is shown in **c**. Data are represented as mean ± sem. *ns* not statistically significant. **d** Immobility time of the mice during the tail suspension tests (each mouse was tested for 5 min) ($n=9$ for the control and 12 for the KO). **e–g** Accelerated rotarod tests of 4-month-old ($n=9$ for control and 5 for KO), 6-month-old ($n=14$ for control and 13 for KO) and 11-month-old ($n=14$ for control and 13 for KO) mice as indicated. Mice were tested four times per day (with a 20-min break between 2 trials) for four consecutive days. The average of the four repeats in each day was calculated as the latency time for each mouse on that day. **h** Latency time of the mice on the 4th day is shown for 4-, 6-, and 11-month-old mice. *$p<0.05$. The p values for all the time points are shown, no matter whether they are statistically significant or not. For graphs in **e–h**, "latency time" refers to the duration during which the mice stayed on the rotarod

lack of coordination and increased mental abnormalities at advanced stages. Tubulin acetylation is associated with Huntington's disease, and levels of tubulin acetylation are reduced in patients' brains [10]. Many studies associated HDAC6 with Huntington's disease [10, 36–38]. As HDAC6 is the major tubulin deacetylase, tubulin acetylation might have a role in Huntington's disease. Our study on ATAT1 established a link between tubulin acetylation loss and hypoplasia in the striatum. Inhibition of HDAC6 increases the transport of the cortico-striatal derived neurotrophic factor BDNF through elevated tubulin acetylation [10]. BDNF is neuroprotective for striatal neurons both in vitro and in vivo.

It seems possible that tubulin acetylation affects the striatum through regulation of BDNF. However, in another study, it was shown that elevated tubulin acetylation levels did not affect the efficiency of BDNF transport from the cortex to the striatum [39]. The role of tubulin acetylation in BDNF transport requires further investigation.

Tubulin acetylation is important for touch sensitivity in *C. elegans* [16]. A recent study showed that tubulin acetylation is also essential for touch sensation in mice [23]. Loss of MEC-17 and tubulin acetylation has been shown to disrupt microtubule organization [7, 8]. However, none of these proposed functions of tubulin acetylation affect mouse development significantly. We observed hypoplasia in the striatum and septum, but it did not affect mouse survival as well. A recent study showed that ATAT1 are critical for cell proliferation, as cell growth rate increased > five folds in the absence of *Atat1* [40]. Reported in another study, genetic disruption of *Atat1* inhibits proliferation and invasion of colon cancer cells, while restoring the levels of ATAT1 in *Atat1*-deficient cells restores the cancer cell invasive characteristics [41]. These two studies showed contradicting roles of ATAT1 in regulating cell proliferation. With *Atat1*$^{-/-}$ MEFs, we observed only a slight increase in proliferation for the first few days (Fig. 7b). Whether the role of tubulin acetylation in proliferation is dependent on cell types and their growing environment needs further investigation.

The lack of major phenotypes in *Atat1*-null mutant mice suggests that this enzyme may be important under adverse conditions. Related to this, one important development about tubulin acetylation is its role in regulating stress responses. It was recently shown that stimuli such as exposure to a higher concentration of NaCl could induce tubulin hyperacetylation [42]. This observation implies that tubulin acetylation might have a role in stress responses. As reported [42], we observed that stressing stimuli such as treatment with high concentration of NaCl induces tubulin hyperacetylation in wild-type MEFs (Fig. 7). Interestingly, no tubulin acetylation was observed in *Atat1*$^{-/-}$ MEFs with or without the stimuli (Fig. 7), indicating that ATAT1 is dispensable for tubulin hyperacetylation upon exposure to high salt. Importantly, ATAT1 is also dispensable for tubulin hyperacetylation upon exposure to high glucose and oxidative stresses such as H_2O_2 exposure. These stress conditions are related to various human diseases. High salt consumption (e.g., associated with Western lifestyle) predisposes individuals to hypertension and cardiovascular disease, as well as autoimmunity [43], whereas high blood sugar is a hallmark of diabetes mellitus. Thus, it will be important to investigate how ATAT1 plays a role under these pathological conditions. Tubulin hyperacetylation upon exposure to high salt may be due to acute activation of TAK1, which is osmotic inducible and activates ATAT1 rapidly [40], or salt-inducible kinases [43, 44]. Microtubule hyperacetylation could also be induced by lipopolysaccharide treatment. Such induced acetylation is found to be necessary for production of the anti-inflammatory cytokine IL-10 [45]. Related to this, tubulin is hyperacetylated in response to IFNγ treatment [45]. Different from this, tubulin acetylation is inhibited by chondroitin sulfate proteoglycans and myelin-associated glycoprotein [46]. Two recent studies have shown that tubulin acetylation enhances flexibility of microtubules under physical pressure [47, 48]. Therefore, it will be important to elucidate the role of ATAT1 and tubulin acetylation in cell signaling events related to stress responses and different pathogenic processes.

Atat1 is highly expressed in ciliated tissues such as ependymal cells of the lateral ventricle (Fig. 1d), the nasal cavity and the ganglion cell layer of the eyes (Fig. 9d). While tubulin acetylation is found lost in ependymal cilia (Fig. 1e), residual levels were detected in the trachea, oviduct, thymus and spleen (Fig. 9). These results indicate that while ATAT1 is the acetyltransferase governing tubulin acetylation in the brain and many other tissues [21, 22], there may be another tubulin acetyltransferase in certain tissues such as the trachea, oviduct, thymus and spleen (Fig. 9). Prior to identification of ATAT1, three other enzymes were reported to possess tubulin acetyltransferase activity [28, 49–51]. It will be interesting to investigate whether any one of them or another protein is responsible for the residual tubulin acetylation observed in the heart, skeletal muscle, trachea, oviduct, thymus and spleen (Fig. 9).

The role of *Atat1* in the blood system remains unclear [21, 22]. Our analysis of hematopoietic cells did not yield any obvious defects (Tables 1, 2; Fig. 8), suggesting minimal roles of ATAT1 in regulating hematopoiesis. However, HDAC6 is important for regulating platelet maturation and activation [52, 53]. Platelets are important in hemostasis and thrombosis, so they are highly relevant to different clinical conditions such as hypercholesterolemia [54]. In addition, platelet overproduction is characteristic of essential thrombocythemia, a rare chronic blood condition [55]. Thus, it remains to be investigated whether ATAT1 plays a role in modulating such pathological processes.

This study thus identifies ventricular dilation along with septal and striatal hypoplasia as major phenotypes in *Atat1*-null mice and demonstrates that ATAT1 is essential for acute tubulin hyperacetylation in stress responses. No patients with germline *ATAT1* mutations have been reported yet, but the forebrain defects in the mice should help identify and characterize such mutations. Search through the Genematcher Web server [56] has not yielded any viable candidates yet. About patient identification, it is noteworthy that such patients (if any) may have more prominent phenotypes than what has been observed in the mutant mice, just as we have recently shown for patients with heterozygous mutations of another gene [57]. In sum, in addition to

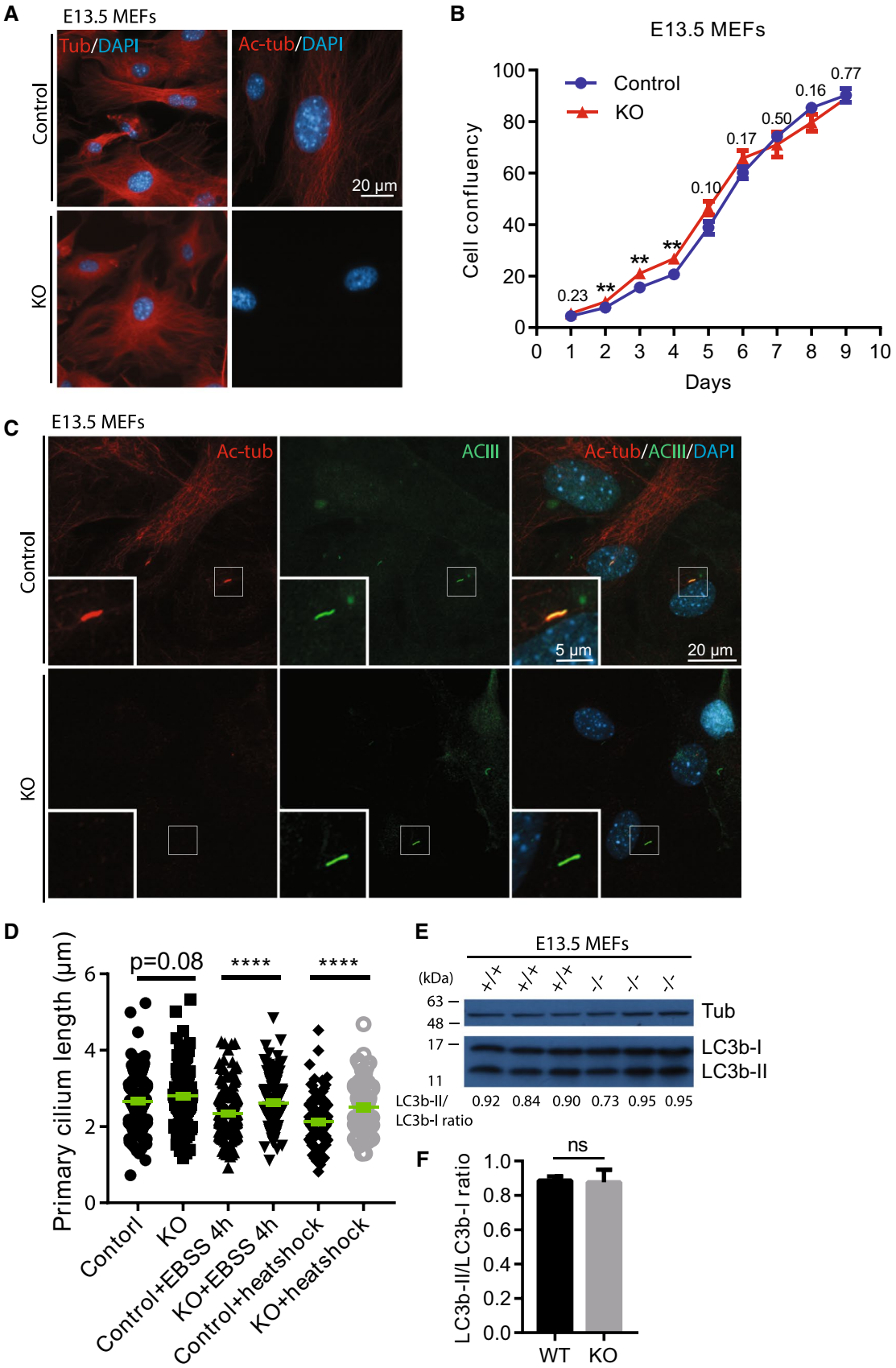
A
E13.5 MEFs
Tub/DAPI
Ac-tub/DAPI
Control
KO
20 μm
B
E13.5 MEFs
Control
KO
Cell confluency
Days
0.23
0.10
0.17
0.50
0.16
0.77
**
C
E13.5 MEFs
Ac-tub
ACIII
Ac-tub/ACIII/DAPI
Control
KO
5 μm
20 μm
D
Primary cilium length (μm)
p=0.08
****
Contorl
KO
Control+EBSS 4h
KO+EBSS 4h
Control+heatshock
KO+heatshock
E
E13.5 MEFs
(kDa)
+/+
-/-
63
48
17
11
Tub
LC3b-I
LC3b-II
LC3b-II/ LC3b-I ratio
0.92 0.84 0.90 0.73 0.95 0.95
F
ns
LC3b-II/LC3b-I ratio
WT
KO

◂**Fig. 6** *Atat1 l*oss slightly affects growth and other characteristics of MEFs. **a** Immunofluorescence microscopy to detect α-tubulin and its acetylation in MEFs prepared from wild-type and *Atat1*$^{-/-}$ embryos at E13.5. Note that the acetylation is detectable in the wild-type but not mutant MEFs. **b** Growth curves of control and *Atat1*$^{-/-}$ MEFs measured by an IncuCyte imaging system ($n=4$). The p values are indicated for the time points when the difference was not statistically significant. $^{**}p<0.01$. **c** Primary cilia in MEFs detected by immunostaining with anti-ACIII and anti-acetyl-tubulin antibodies. Immunofluorescence microscopic images of primary cilia were enlarged and shown at the bottom-left corners. **d** Length of primary cilia in regular MEFs and those with EBSS treatment or heat shock. For each group, 50–200 primary cilia were measured. **e** Western blotting with the LC3b I/II antibody to detect autophagy in wild-type and *Atat1*$^{-/-}$ MEFs. **f** The LC3b-II/LC3b-I ratio (indicative of autophagy) is not affected ($n=3$). All quantitative data are represented as mean ± sem; ns, not statistically significant; $^{**}p<0.01$; $^{****}p<0.0001$

the forebrain defects and the lack of stress-induced tubulin hyperacetylation, this study provides evidence suggesting the existence of a new α-tubulin acetyltransferase, thereby guiding us for further research on the function and regulation of tubulin acetylation, a post-translation modification that is conserved from lower organisms to humans.

Experimental procedures

Animals and mouse genotyping

Atat1$^{-/-}$ mice were obtained from the Knockout Mouse Project (KOMP) repository (Project ID: VG14032), as previously described [21]. The DNA fragment between the first last exons was replaced by a cassette containing a promoter-less *LacZ* transgene and a *Neo* gene [21]. The cassette was flanked by two LoxP sites, and removal of this cassette between two LoxP sites had no impact on the mutant phenotype. Mice were on the C57BL/6J background and maintained in the animal facility of Goodman Cancer Centre of McGill University. All procedures involved in the experiments relating to mice were performed according to the guidelines and protocols approved by the McGill Animal Use Committee.

Tissue extract preparation and Western blotting

Tissues were taken from 2-month-old littermates of wild-type and *Atat1*$^{-/-}$ mice. Tissues were weighted and homogenized with a plastic pestle in Eppendorf tubes by adding 3 volumes of the RIPA buffer (25 mM Tris–HCl pH 7.6, 150 mM NaCl, 1% nonidet P-40, 1% sodium deoxycholate, and 0.1% SDS, supplemented with a protease inhibitor cocktail composed of phenylmethylsulfonyl fluoride, aprotinin, pepstatin and leupetin). After additional homogenization by sonication with a Virsonic 100 sonicator (Virtis, Inc) at setting 5 for six times (5 s each), the suspension was centrifuged at ~ 20,000*g* and 4 °C for 10 min. The supernatant was collected as the soluble tissue protein extract. 1 µl of the protein extract was used for protein concentration measurement by a Bradford assay kit (Bio-Rad) and the rest was flash-frozen in a dry ice–methanol bath for further storage at − 80 °C.

For Western blotting, tissue extracts were mixed with a 3 × reducing sample buffer (188 mM Tris–HCl pH 6.8, 6% SDS, 30% glycerol, 0.3% bromophenol blue and 16% β-mercaptoethanol) and boiled for 5–8 min before SDS-PAGE and immunoblotting. The membranes were blocked in a 0.15% Tween-20/PBS solution containing 5% non-fat skimmed milk at room temperature for 0.5–1 h, with agitation. Primary antibodies were then added: anti-α-tubulin antibody (Sigma, T5168; 1:2500 dilution), anti-acetylated tubulin (Sigma, T7451, clone 6-11B-1; 1:5000) and anti-LC3b I/II antibody (Novusbio, NB100-2220; 1:1000). After further incubation overnight at 4 °C with slight agitation, the membranes were washed three times, 10 min each, and incubated with the blocking solution containing the horseradish peroxidase-conjugated sheep anti-mouse IgG secondary antibody (GE Healthcare Life Sciences, NA931 V; diluted at 1:5000) for 1 h. After three washes, 10 min each, protein bands were labeled with the WEST-ZOL plus Western Blot Detection System (iNtRON Biotechnology, Seoul, Korea) for subsequent exposure to X-ray films.

MEF isolation and culture

MEFs were isolated from mouse embryos, which were dissected out of pregnant mice at E13.5. The head and internal organs of the embryos were removed. The remaining parts were minced with scissors and digested with 0.25% Trypsin–EDTA for 10 min with shaking in a 37 °C shaker. After centrifugation at room temperature, the supernatant was removed and the pellet was resuspended in a complete medium containing DMEM supplemented with 15% fetal bovine serum, non-essential amino acids (Thermo Fisher Scientific, Cat No. 11140050), penicillin and streptomycin (Thermo Fisher Scientific, Cat No. 15140122)). The cell suspension was cultured in a low oxygen incubator (4% O_2). MEF protein extraction and Western blotting were carried out as described above for mouse tissue extracts.

Frozen section preparation

Mice were anesthetized and perfused first with 50 ml cold PBS and then with 50 ml cold 2% PFA in PBS, as previously described [21]. The brains were then dissected out under a hood. For embryos, whole embryos or their brains were collected. The tissues were fixed at 4 °C for 2–16 h in the fixative solution [0.1 M phosphate buffer (pH 7.4), 2% PFA, 0.2% glutaraldehyde, 5 mM EGTA (pH 8.0), 2 mM $MgCl_2$

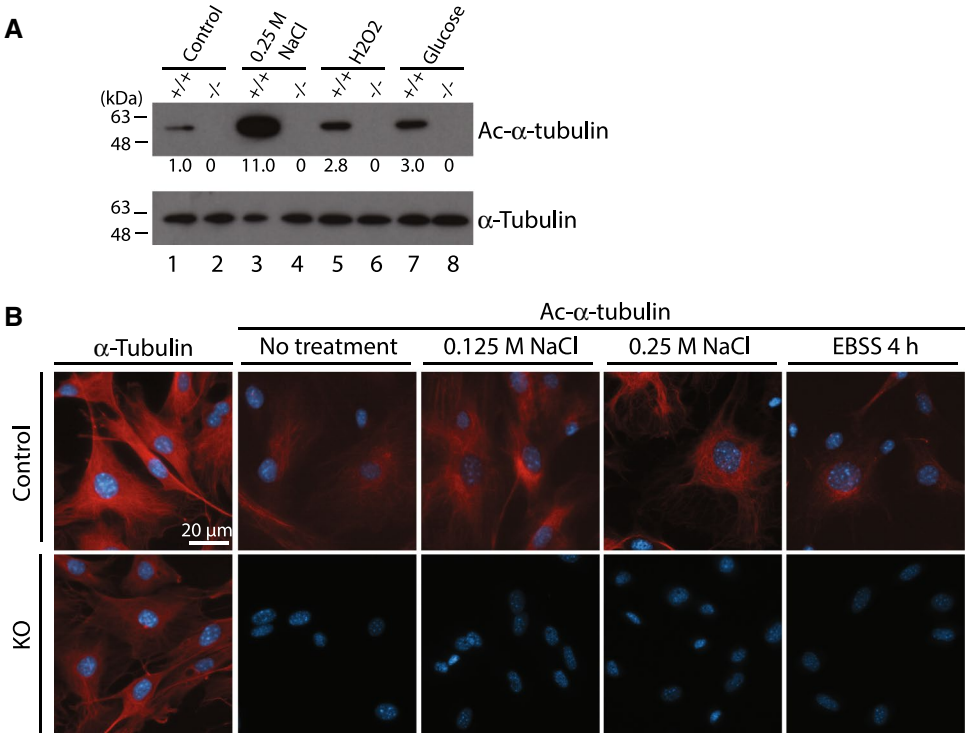

Fig. 7 Disappearance of stress-induced tubulin hyperacetylation in *Atat1*$^{-/-}$ MEFs. **a** Western blots showing that treatment with 0.25 M NaCl, 5 mM H_2O_2 or 100 mM glucose for 30 min stimulated tubulin hyperacetylation in the wild-type but not mutant MEFs. The relative acetylation levels are indicated at the bottom of the upper panel, with that on lane 1 being arbitrarily set to 1.0. Note that in DMEM media, the regular concentration of NaCl is 58 mM while and the glucose concentration is either 5.5 or 25 mM. **b** Immunofluorescence microscopic analysis with anti-α-tubulin and -acetyl-α-tubulin antibodies confirmed that NaCl treatment stimulated tubulin hyperacetylation in the wild-type but not mutant MEFs

Table 1 Complete blood counts for control and *Atat1*-null mice

	Control	Knockout	Significance
Erythroid			
RBCs, × 10^{12}/L	8.8 ± 0.6	9.0 ± 0.9	ns
MCV, fL	44.7 ± 0.5	46.0 ± 0.7	ns
Hemoglobin, g/L	138.3 ± 7.9	141.0 ± 13.4	ns
Hematocrit, L/L	0.4 ± 0.03	0.42 ± 0.04	ns
MCH, pg	15.7 ± 0.3	15.7 ± 0.2	ns
MCHC, g/L	350.0 ± 7.5	340.8 ± 4.6	ns
Leukocytes			
WBCs, × 10^9/L	2.6 ± 1.1	3.6 ± 1.1	ns
Neutrophils, %	15.3 ± 9.8	12.0 ± 3.5	ns
Lymphocytes, %	67.0 ± 16.9	86.0 ± 3.4	ns
Monocytes, %	0.0 ± 0.0	0.3 ± 0.4	ns
Eosinophils, %	1.0 ± 0.8	1.5 ± 0.5	ns
Platelets, × 10^9/L	345.7 ± 272.3	865.5 ± 83.0	ns[a]

Values represent mean ± SD, calculated from three wild-type and four knockout mice at 2 months of age. *ns* not statistically significant

RBC red blood cells, *MCV* mean corpuscular volume, *MCH* mean corpuscular hemoglobin, *MCHC* mean corpuscular hemoglobin concentration, *WBC* white blood cell

[a]There was apparent increase of platelet production in these mutant mice, but analysis of three additional pairs revealed no overall statistical difference, which is also consistent with what was reported in a previous study [22]

and 0.2% Nonidet-P40] and subsequently equilibrated first with 15% sucrose in PBS for 8 h and then with 30% sucrose in PBS overnight at 4 °C till the tissues sunk to the bottom of the container. The tissues were taken out from the fixative solution and blotted with wipe tissue paper to remove extra solution. Afterward, the tissues were incubated with the OCT compound (Tissue-Tek) in cassettes at 4 °C for 30 min. After the tissue orientation was adjusted as desired, the cassette was snap-frozen in a dry ice–methanol bath. The blocks were sectioned on a cryostat (Thermo Shandon, A77210167), and 15-μm sections were collected onto glass slides (Fisher Scientific). The sections were air-dried at room temperature for ~ 1 h for storage at − 80 °C.

β-Galactosidase staining of frozen sections

Frozen sections were taken out from a − 80 °C freezer and put at room temperature for 10 min to thaw. The sections were then post-fixed in a fixative (0.2% PFA in 0.1 M PIPES, pH 6.9, 2 mM $MgCl_2$, and 5 mM EGTA) on ice for 10 min, then rinsed and washed in PBS containing 2 mM $MgCl_2$ for 10 min. Sections were permeabilized by incubation in the detergent solution (PBS containing 0.3% Triton X-100) on ice for 10 min, and then changed to the β-gal staining solution [21] and incubated at 37 °C in the dark until the desired color was reached (varying from 1 h to overnight). The slides were then washed in PBS containing 2 mM $MgCl_2$ three times, 5 min each, followed by washing in distilled water for 5 min. Sequential dehydration was performed with 70, 95

Table 2 Biochemical analysis of blood from control and *Atat1*-null mice

	Units	Control	Knockout	Significance
Total protein	g/L	52 ± 1	50.25 ± 1.3	ns
Albumin	g/L	26 ± 0	25.5 ± 1.1	ns
Albumin/globulin ratio		1 ± 0	1.05 ± 0.05	ns
Glucose	mmol/L	11 ± 0.8	17.6 ± 5.1	ns
BUN urea	mmol/L	7.8 ± 0.3	7.45 ± 0.78	ns
Creatinine	μmol/L	7 ± 0	11.25 ± 0.83	ns
Total bilirubin	μmol/L	20.5 ± 4.5	12.25 ± 2.95	ns
ALT	U/L	34.5 ± 1.5	50.5 ± 5.89	ns
AST	U/L	209.5 ± 2.5	149.5 ± 26.51	ns
Alkaline phosphatase	U/L	69.5 ± 17.5	87 ± 3.08	ns
GGT	U/L	14[a]	NA	NA
CK	U/L	753.5 ± 49.5	394 ± 120.35	ns
Cholesterol	mmol/L	2.865 ± 0.135	3.05 ± 0.28	ns
Sodium	mmol/L	154[a]	153.3 ± 1.8	NA
Potassium	mmol/L	7.1[a]	8.325 ± 3.05	NA
Chloride	mmol/L	115[a]	112.5 ± 1.12	NA
Calcium	mmol/L	2.36 ± 0.09	2.65 ± 0.07	ns
Phosphorus	mmol/L	3.31 ± 0.17	3.57 ± 0.39	ns
Magnesium	mmol/L	1.535 ± 0.025	1.62 ± 0.10	ns

Values represent mean ± SD, calculated from two wild-type and four knockout mice at 2 months of age

ns not statistically significant, *NA* not available, *BUN* blood urea nitrogen, *ALT* alanine aminotransferase, *AST* aspartate aminotransferase, *GGT* gamma-glutamyl transferase, *CK* creatine kinase

[a]Value from one WT mouse as value from another one is not available

and 100% ethanol (5 min each). Sections were incubated in xylene twice, 5 min each, and mounted with the ClearMount mounting medium (American Master Tech, MM0126).

BrdU labeling and paraffin section preparation

BrdU was injected intraperitoneally into E13.5 pregnant mice or P10 mice at a dose of 50 μg BrdU per gram of body weight as previously described [58, 59]. For cell tracking, after BrdU injection into E13.5 pregnant mice, brains of the new pups were collected at P10. For S-phase cell analysis, and brains of the P10 mice were collected 1 h after BrdU injection. The collected brains were fixed in 4% paraformaldehyde (PFA) overnight, followed by paraffin processing and embedding. The paraffin blocks were sectioned on a Leica Rotary Microtome (Leica RM2125RTS). 5-μm sections were collected onto glass slides (Fisher Scientific) and baked 2 h at 37 °C. The slides were kept at 4 °C for long-term storage.

Histological analysis and immunostaining of brain sections

For histological analysis, Nissl staining was carried out as described previously [21, 58, 59]. For immunohistochemical staining of BrdU, the paraffin sections were dewaxed, rehydrated and exposed to 2 N HCl at 37 °C for 30–60 min before antigen retrieval by boiling in 10 mM of sodium citrate (pH 6.0) for 20 min. After cooldown, sections were incubated in blocking buffer (2% BSA in 0.2% Triton X-100/PBS solution) at room temperature for 30–60 min before incubation with a rat anti-BrdU antibody (Abcam, AB6326, 1:200) in the blocking buffer at 4 °C overnight. After washing twice in 0.2% Triton/PBS, sections were incubated with biotin-SP-conjugated AffiniPure donkey-anti-rat IgG(H + L) antibody (Jackson ImmunoResearch, 712-065-153, 1:500). The signal was developed with the Vector ABC and DAB substrate kits (Vector Labs, PK-4001, SK-4100). For immunofluorescence staining, after deparaffinization, rehydration and antigen retrieval, the sections were incubated in blocking buffer for 30–60 min, followed by incubation with primary antibodies overnight at 4 °C and secondary antibodies for 1 h at room temperature [21]. The following antibodies were used: goat-anti-Sox2 (R&D systems, AF2018, 1:200), rabbit anti-Tbr2 (Abcam, ab23345, 1:400), rabbit anti-Cux1 (1:200) [60], rat anti-Ctip2 (Abcam, ab18465, 1:400), rabbit anti-Cux2 (1:200) [61], rabbit anti-Tbr1 (1:400), mouse anti-α-tubulin antibody (Sigma, T5168, 1:1000), mouse anti-acetylated tubulin (Sigma, T7451, clone 6-11B-1, 1:1000), rabbit anti-ACIII (Abcam, ab125093, 1:1000), Alexa Fluor 488-conjugated goat-anti-rabbit IgG (Invitrogen, A-11008, 1:500), Alexa Fluor 488-conjugated donkey-anti-goat IgG

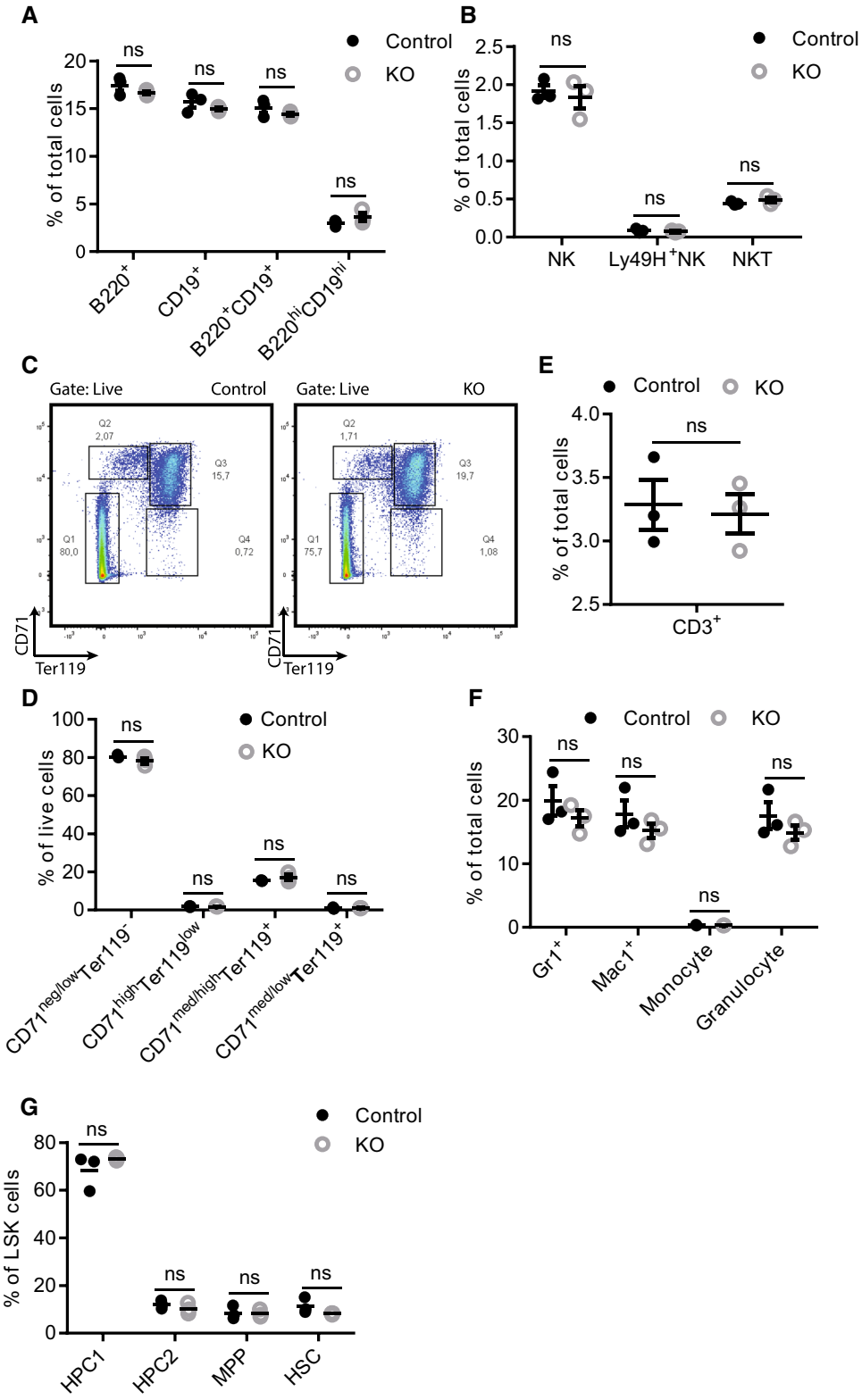

Fig. 8 Cytometric analysis of various wild-type and *Atat1*$^{-/-}$ bone marrow cells. **a** Percentage of B220^{+}, CD19^{+}, B220^{+}CD19^{+} and B220^{hi}CD19^{hi} cells in total nucleated cells from wild-type and mutant bone marrows. Young adult mice at the age of 2 months were used. **b** Percentage of NK (NK1.1^{+}CD3^{-}), Ly49H^{+} NK and NKT cells (NK1.1^{+}CD3^{+}) in total nucleated cells from wild-type and mutant bone marrows. **c** Gating of nucleated cells from wild-type and mutant bone marrows using CD71 and Ter119 antibodies. **d** Quantification of cell populations shown in **c**. **e** Percentage of CD3^{+} cells in total nucleated cells from wild-type and mutant bone marrows. **f** Percentage of Gr1^{+} cells, Mac1^{+} cells, monocytes (Gr1^{lo}Mac1^{hi}) and granulocytes (Gr1^{hi}Mac1^{h}) in the total nucleated cells from wild-type and mutant bone marrows. **g** Ratio of hematopoietic stem and progenitor cells (HSC, HPC1, HPC2 and MPP) in total LSK (Lin^{-}Sca1^{+}c-Kit^{+}) cells. HSC, LSKCD48^{-}CD150^{+}; HPC1, LSKCD48^{+}CD150^{-}; HPC2, LSKCD48^{+}CD150^{+}; MPP, LSKCD48^{-}CD150^{-}; $n=3$ for all groups. The cell marker abbreviations are used as previously described [65]. All data are represented as mean ± sem; *ns* not statistically significant

(Invitrogen, A-11055, 1:500), Alexa Fluor 568-conjugated goat-anti-rabbit IgG (Invitrogen, A-11011, 1:500), Alexa Fluor 488-conjugated goat-anti-rat IgG (Invitrogen, A-11006, 1:500) and Alexa Fluor 568-conjugated goat-anti-mouse IgG (Invitrogen, A-11004, 1:500). Golgi staining was carried out as described [62]. TUNEL assays were performed with the DeadEnd™ Fluorometric TUNEL System (Promega, G3250).

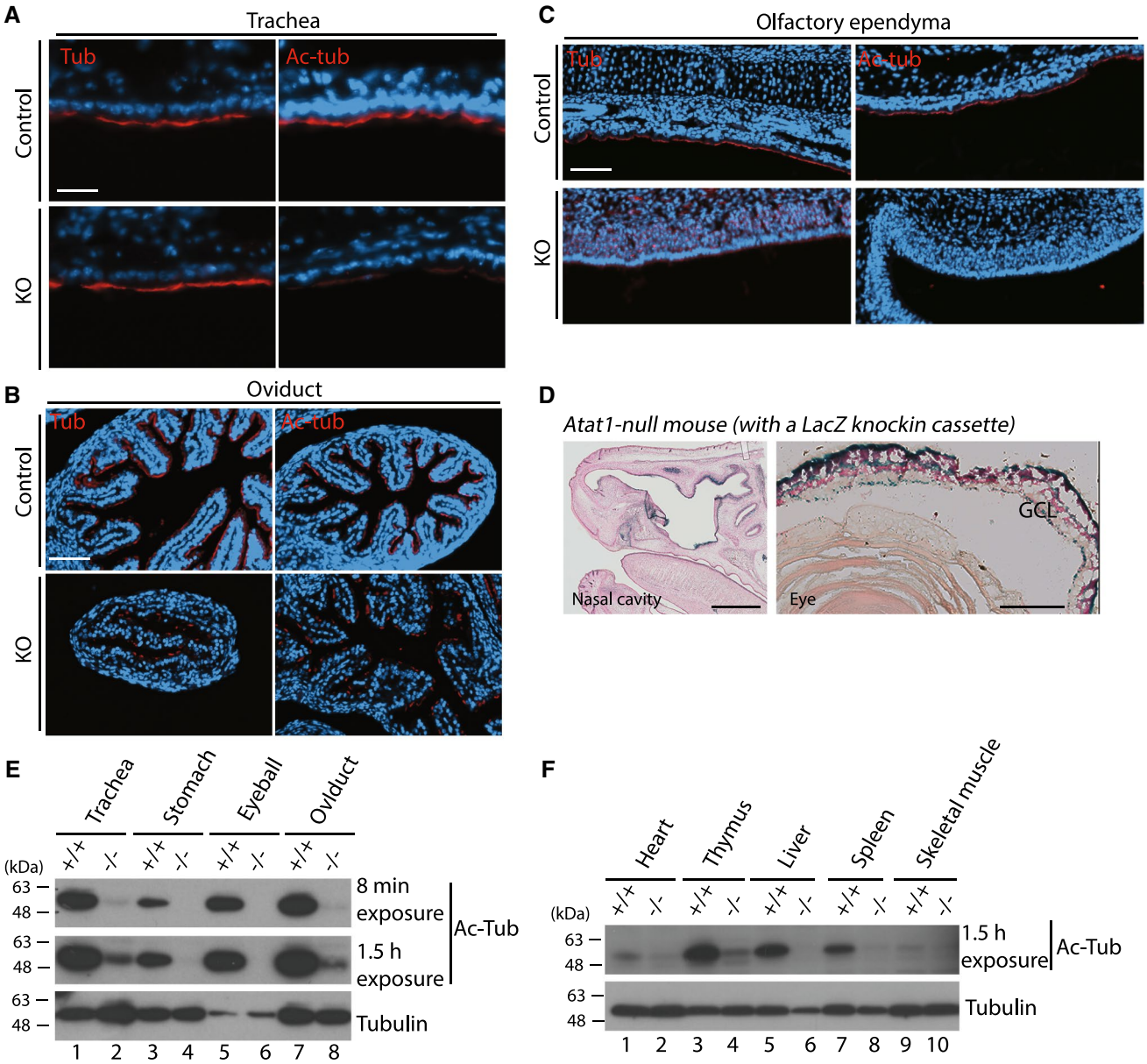

Fig. 9 Residual tubulin acetylation in some tissues of the *Atat1*$^{-/-}$ mice. **a**–**c** Immunofluorescence microscopic analysis with anti-tubulin (Tub) and -acetyl-tubulin (Ac-Tub) antibodies of the trachea, oviduct and olfactory ependyma sections. Scale bars, 30 µm (**a**) and 50 µm (**b**, **c**). **d** β-Gal staining of sagittal head sections from *Atat1*$^{-/-}$ mice at P0, as carried out as in Fig. 1d. These particular mice still contained a promoter-less LacZ cassette inserted at the *Atat1* locus [21]. Scale bars, 1 mm for the nasal cavity and 200 µm for the eye. **e**, **f** Detection of tubulin and acetylated tubulin by Western blotting in various tissue extracts

Behavioral tests

The open field test was carried out in a 40 × 40 × 40 cm arena box as described [63]. Briefly, the cages with mice were taken to a quiet testing room 1 h before the experiment started. Each mouse was put at the center of the arena and recorded for 10 min while disturbance during the whole testing process was avoided. Between each test, the bottom of the box was cleaned with 75% alcohol and paused for 5 min before starting the next test. The recorded videos were analyzed by the SMART 3.0 video-tracking system (Pan-Lab, Harvard Apparatus).

Rotarod tests were carried out with an accelerating rotarod protocol as described [29]. Mice were placed on a rotarod (Stoelting Europe). The rod was accelerated from 4 to 40 rpm in 5 min, and then maintained at 40 rpm for 5 min. The latency to fall was recorded for each mouse as an indicator for motor coordination. Each mouse was tested four times per day, with at least a 20-min break between two trials. All the mice were tested for four consecutive days.

For the tail suspension test, cages with mice were brought to a quiet testing room where the experiment was carried out 1 h before the experiment started. Each mouse was suspended by the tail for 5 min and recorded with a video camera while disturbance during the test was avoided. Afterward, the immobile time (as an indicator for depression) was measured from the recorded videos.

Complete blood counting and flow cytometry

For complete blood counting, whole blood was collected into tubes containing anticoagulants via heart puncture from anesthetized 2-month-old mice as described [64]. The whole blood was then sent to the blood testing laboratory at the Comprehensive Animal Center of McGill University for complete blood counting. Multicolor flow cytometry was carried out as described [65]. Specifically, bone marrows were flushed out from femurs and tibias with DMEM containing 2% FBS. The bone marrows were pipetted up and down with a 1-ml tip and then passed through a 40-µm cell strainer (StemCell Technologies). Red blood cells were removed using the Red Blood Cell (RBC) Lysis Buffer (eBioscience). FVD-eFluor 506 (eBioscience) was used for labeling dead cells, which were excluded during flow cytometric analysis. Cell surface markers, such as CD3, B220, Gr1, Ter119 and Mac1 (all from eBioscience), were used for labeling lineage-specific cells. For hematopoietic stem and progenitor cells, lineage markers were combined with four additional cell surface markers, Scal1, cKit, CD48 and CD150. The labeled cells were analyzed with a BD FACSAria sorter and analyzed by FlowJo software (Treestar).

Statistical analysis

Statistical analysis was performed with unpaired two-tailed Student's *t* test. $p < 0.05$ was considered to be statistically significant. Graphs were generated with GraphPad Prism 6 (GraphPad Software).

Acknowledgements This work was supported by research grants from Canadian Institutes of Health Research, Natural Sciences and Engineering Research Council of Canada and the Canadian Cancer Society (to X.-J.Y.). L.L. received stipend support from the China Scholarship Council, the Clifford C.F. Wong Fellowship program, a CIHR/FRSQ training grant in cancer research for the McGill Integrated Cancer Research Training Program and the Canderel Foundation.

Author contributions LL carried out all experiments and wrote the manuscript; SJ and AW supervised the rotarod tests; MM helped perform some experiments with MEFs; LML and SM assisted with open field tests; XJY supervised the project and finalized the manuscript.

Compliance with ethical standards

Conflict of interest The authors declare no conflicts of interest with the contents of this study.

References

1. Lhernault SW, Rosenbaum JL (1985) Chlamydomonas alpha-tubulin is posttranslationally modified by acetylation on the epsilon-amino group of a lysine. Biochemistry 24:473–478
2. Ledizet M, Piperno G (1987) Identification of an acetylation site of chlamydomonas alpha-tubulin. Proc Natl Acad Sci USA 84:5720–5724
3. Piperno G, Ledizet M, Chang XJ (1987) Microtubules containing acetylated alpha-tubulin in mammalian-cells in culture. J Cell Biol 104:289–302
4. Piperno G, Fuller MT (1985) Monoclonal-antibodies specific for an acetylated form of alpha-tubulin recognize the antigen in cilia and flagella from a variety of organisms. J Cell Biol 101:2085–2094
5. Nakagawa U, Suzuki D, Ishikawa M, Sato H, Kamemura K, Imamura A (2013) Acetylation of alpha-Tubulin on Lys(40) is a widespread post-translational modification in angiosperms. Biosci Biotech Bioch 77:1602–1605
6. Yang XJ, Grégoire S (2005) Class II histone deacetylases: from sequence to function, regulation and clinical implication. Mol Cell Biol 25:2873–2884
7. Topalidou I, Keller C, Kalebic N, Nguyen KCQ, Somhegyi H, Politi KA, Heppenstall P, Hall DH, Chalfie M (2012) Genetically separable functions of the MEC-17 tubulin acetyltransferase affect microtubule organization. Curr Biol 22:1057–1065
8. Cueva JG, Hsin J, Huang KC, Goodman MB (2012) Posttranslational acetylation of alpha-tubulin constrains protofilament number in native microtubules. Curr Biol 22:1066–1074
9. Reed NA, Cai DW, Blasius TL, Jih GT, Meyhofer E, Gaertig J, Verhey KJ (2006) Microtubule acetylation promotes kinesin-1 binding and transport. Curr Biol 16:2166–2172
10. Dompierre JP, Godin JD, Charrin BC, Cordelieres FP, King SJ, Humbert S, Saudou F (2007) Histone deacetylase 6 inhibition compensates for the transport deficit in Huntington's disease by increasing tubulin acetylation. J Neurosci 27:3571–3583
11. Hubbert C, Guardiola A, Shao R, Kawaguchi Y, Ito A, Nixon A, Yoshida M, Wang XF, Yao TP (2002) HDAC6 is a microtubule-associated deacetylase. Nature 417:455–458
12. Zhang Y, Li N, Caron C, Matthias G, Hess D, Khochbin S, Matthias P (2003) HDAC-6 interacts with and deacetylates tubulin and microtubules in vivo. EMBO J 22:1168–1179
13. Matsuyama A, Shimazu T, Sumida Y, Saito A, Yoshimatsu Y, Seigneurin-Berny D, Osada H, Komatsu Y, Nishino N, Khochbin S, Horinouchi S, Yoshida M (2002) In vivo destabilization of dynamic microtubules by HDAC6-mediated deacetylation. EMBO J 21:6820–6831
14. Zhang Y, Kwon S, Yamaguchi T, Cubizolles F, Rousseaux S, Kneissel M, Cao C, Li N, Cheng HL, Chua K, Lombard D, Mizeracki A, Matthias G, Alt FW, Khochbin S, Matthias P (2008) Mice lacking histone deacetylase 6 have hyperacetylated tubulin but are viable and develop normally. Mol Cell Biol 28:1688–1701
15. Janke C, Montagnac G (2017) Causes and consequences of microtubule acetylation. Curr Biol 27:R1287–R1292
16. Akella JS, Wloga D, Kim J, Starostina NG, Lyons-Abbott S, Morrissette NS, Dougan ST, Kipreos ET, Gaertig J (2010) MEC-17 is an alpha-tubulin acetyltransferase. Nature 467:218–222

17. Shida T, Cueva JG, Xu ZJ, Goodman MB, Nachury MV (2010) The major alpha-tubulin K40 acetyltransferase alpha TAT1 promotes rapid ciliogenesis and efficient mechanosensation. Proc Natl Acad Sci USA 107:21517–21522
18. Li L, Wei D, Wang Q, Pan J, Liu R, Zhang X, Bao L (2012) MEC-17 deficiency leads to reduced alpha-tubulin acetylation and impaired migration of cortical neurons. J Neurosci 32:12673–12683
19. Boggs AE, Vitolo MI, Whipple RA, Charpentier MS, Goloubeva OG, Ioffe OB, Tuttle KC, Slovic J, Lu YL, Mills GB, Martin SS (2015) alpha-tubulin acetylation elevated in metastatic and basal-like breast cancer cells promotes microtentacle formation, adhesion, and invasive migration. Cancer Res 75:203–215
20. Li L, Yang XJ (2015) Tubulin acetylation: responsible enzymes, biological functions and human diseases. Cell Mol Life Sci 72:4237–4255
21. Kim GW, Li L, Ghorbani M, You L, Yang XJ (2013) Mice lacking alpha-tubulin acetyltransferase 1 are viable but display alpha-tubulin acetylation deficiency and dentate gyrus distortion. J Biol Chem 288:20334–20350
22. Kalebic N, Sorrentino S, Perlas E, Bolasco G, Martinez C, Heppenstall PA (2013) alphaTAT1 is the major alpha-tubulin acetyltransferase in mice. Nat Commun 4:1962
23. Morley SJ, Qi YM, Iovino L, Andolfi L, Guo D, Kalebic N, Castaldi L, Tischer C, Portulano C, Bolasco G, Shirlekar K, Fusco CM, Asaro A, Fermani F, Sundukova M, Matti U, Reymond L, De Ninno A, Businaro L, Johnsson K, Lazzarino M, Ries J, Schwab Y, Hu J, Heppenstall PA (2016) Acetylated tubulin is essential for touch sensation in mice. Elife 5
24. Howes SC, Alushin GM, Shida T, Nachury MV, Nogales E (2014) Effects of tubulin acetylation and tubulin acetyltransferase binding on microtubule structure. Mol Biol Cell 25:257–266
25. Lin X, Liu BH, Yang XS, Yue XJ, Diao LX, Wang J, Chang J (2013) Genetic deletion of Rnd3 results in aqueductal stenosis leading to hydrocephalus through up-regulation of Notch signaling. Proc Natl Acad Sci USA 110:8236–8241
26. Banizs B, Pike MM, Millican CL, Ferguson WB, Komlosi P, Sheetz J, Bell PD, Schwiebert EM, Yoder BK (2005) Dysfunctional cilia lead to altered ependyma and choroid plexus function, and result in the formation of hydrocephalus. Development 132:5329–5339
27. Li L, Yang XJ (2015) Tubulin acetylation: responsible enzymes, biological functions and human diseases. Cell Mol Life Sci 72:4237–4255
28. Creppe C, Malinouskaya L, Volvert ML, Gillard M, Close P, Malaise O, Laguesse S, Cornez I, Rahmouni S, Ormenese S, Belachew S, Malgrange B, Chapelle JP, Siebenlist U, Moonen G, Chariot A, Nguyen L (2009) Elongator controls the migration and differentiation of cortical neurons through acetylation of alpha-tubulin. Cell 136:551–564
29. Watt AJ, Cuntz H, Mori M, Nusser Z, Sjostrom PJ, Hausser M (2009) Traveling waves in developing cerebellar cortex mediated by asymmetrical Purkinje cell connectivity. Nat Neurosci 12:463–473
30. Pugacheva EN, Jablonski SA, Hartman TR, Henske EP, Golemis EA (2007) HEF1-dependent Aurora A activation induces disassembly of the primary cilium. Cell 129:1351–1363
31. Prodromou NV, Thompson CL, Osborn DPS, Cogger KF, Ashworth R, Knight MM, Beales PL, Chapple JP (2012) Heat shock induces rapid resorption of primary cilia. J Cell Sci 125:4297–4305
32. Xie R, Nguyen S, McKeehan WL, Liu LY (2010) Acetylated microtubules are required for fusion of autophagosomes with lysosomes. BMC Cell Biol 11:89
33. Banreti A, Sass M, Graba Y (2013) The emerging role of acetylation in the regulation of autophagy. Autophagy 9:819–829
34. Kreitzer AC, Malenka RC (2008) Striatal plasticity and basal ganglia circuit function. Neuron 60:543–554
35. Ma Q, Yang JM, Li T, Milner TA, Hempstead BL (2015) Selective reduction of striatal mature BDNF without induction of proBDNF in the zQ175 mouse model of Huntington's disease. Neurobiol Dis 82:466–477
36. Iwata A, Riley BE, Johnston JA, Kopito RR (2005) HDAC6 and microtubules are required for autophagic degradation of aggregated Huntingtin. J Biol Chem 280:40282–40292
37. Guedes-Dias P, de Proenca J, Soares TR, Leitao-Rocha A, Pinho BR, Duchen MR, Oliveira JMA (2015) HDAC6 inhibition induces mitochondrial fusion, autophagic flux and reduces diffuse mutant huntingtin in striatal neurons. Bba-Mol Basis Dis 1852:2484–2493
38. Simoes-Pires C, Zwick V, Nurisso A, Schenker E, Carrupt PA, Cuendet M (2013) HDAC6 as a target for neurodegenerative diseases: what makes it different from the other HDACs? Mol Neurodegener 8
39. Bobrowska A, Paganetti P, Matthias P, Bates GP (2011) Hdac6 knock-out increases tubulin acetylation but does not modify disease progression in the R6/2 mouse model of huntington's disease. PLoS ONE 6:e20696
40. Shah N, Kumar S, Zaman N, Pan CC, Bloodworth JC, Lei W, Streicher JM, Hempel N, Mythreye K, Lee NY (2018) TAK1 activation of alpha-TAT1 and microtubule hyperacetylation control AKT signaling and cell growth. Nat Commun 9:1696
41. Oh S, You E, Ko P, Jeong J, Keum S, Rhee S (2017) Genetic disruption of tubulin acetyltransferase, alpha TAT1, inhibits proliferation and invasion of colon cancer cells through decreases in Wnt1/beta-catenin signaling. Biochem Bioph Res Co 482:8–14
42. Geeraert C, Ratier A, Pfisterer SG, Perdiz D, Cantaloube I, Rouault A, Pattingre S, Proikas-Cezanne T, Codogno P, Pous C (2010) Starvation-induced hyperacetylation of tubulin is required for the stimulation of autophagy by nutrient deprivation. J Biol Chem 285:24184–24194
43. Wilck N, Matus MG, Kearney SM, Olesen SW, Forslund K, Bartolomaeus H, Haase S, Mahler A, Balogh A, Marko L, Vvedenskaya O, Kleiner FH, Tsvetkov D, Klug L, Costea PI, Sunagawa S, Maier L, Rakova N, Schatz V, Neubert P, Fratzer C, Krannich A, Gollasch M, Grohme DA, Corte-Real BF, Gerlach RG, Basic M, Typas A, Wu C, Titze JM, Jantsch J, Boschmann M, Dechend R, Kleinewietfeld M, Kempa S, Bork P, Linker RA, Alm EJ, Muller DN (2017) Salt-responsive gut commensal modulates TH17 axis and disease. Nature 551:585–589
44. Walkinshaw DR, Weist R, Kim GW, You L, Xiao L, Nie J, Li CS, Zhao S, Xu M, Yang XJ (2013) The tumor suppressor kinase LKB1 activates the downstream kinases SIK2 and SIK3 to stimulate nuclear export of class IIa histone deacetylases. J Biol Chem 288:9345–9362
45. Wang B, Rao YH, Inoue M, Hao R, Lai CH, Chen D, McDonald SL, Choi MC, Wang Q, Shinohara ML, Yao TP (2014) Microtubule acetylation amplifies p38 kinase signalling and anti-inflammatory IL-10 production. Nat Commun 5:3479
46. Wong VSC, Picci C, Swift M, Levinson M, Willis D, Langley B (2018) alpha-Tubulin acetyltransferase is a novel target mediating neurite growth inhibitory effects of chondroitin sulfate proteoglycans and myelin-associated glycoprotein. eNeuro. https://doi.org/10.1523/ENEURO.0240-0217.2018
47. Xu ZJ, Schaedel L, Portran D, Aguilar A, Gaillard J, Marinkovich MP, Thery M, Nachury MV (2017) Microtubules acquire resistance from mechanical breakage through intralumenal acetylation. Science 356:328–332
48. Portran D, Schaedel L, Xu ZJ, Thery M, Nachury MV (2017) Tubulin acetylation protects long-lived microtubules against mechanical ageing. Nat Cell Biol 19:391

49. Solinger JA, Paolinelli R, Kloss H, Scorza FB, Marchesi S, Sauder U, Mitsushima D, Capuani F, Sturzenbaum SR, Cassata G (2010) The *Caenorhabditis elegans* elongator complex regulates neuronal alpha-tubulin acetylation. Plos Genet 6
50. Conacci-Sorrell M, Ngouenet C, Eisenman RN (2010) Myc-nick: a cytoplasmic cleavage product of Myc that promotes alpha-tubulin acetylation and cell differentiation. Cell 142:480–493
51. Ohkawa N, Sugisaki S, Tokunaga E, Fujitani K, Hayasaka T, Setou M, Inokuchi K (2008) *N*-acetyltransferase ARD1-NAT1 regulates neuronal dendritic development. Genes Cells 13:1171–1183
52. Sadoul K, Wang J, Diagouraga B, Vitte AL, Buchou T, Rossini T, Polack B, Xi XD, Matthias P, Khochbin S (2012) HDAC6 controls the kinetics of platelet activation. Blood 120:4215–4218
53. Messaoudi K, Ali A, Ishaq R, Palazzo A, Sliwa D, Bluteau O, Souquere S, Muller D, Diop KM, Rameau P, Lapierre V, Marolleau JP, Matthias P, Godin I, Pierron G, Thomas SG, Watson SP, Droin N, Vainchenker W, Plo I, Raslova H, Debili N (2017) Critical role of the HDAC6-cortactin axis in human megakaryocyte maturation leading to a proplatelet-formation defect. Nat Commun 8:1786
54. Wang N, Tall AR (2016) Cholesterol in platelet biogenesis and activation. Blood 127:1949–1953
55. Krishnegowda M, Rajashekaraiah V (2015) Platelet disorders: an overview. Blood Coagul Fibrinolysis 26:479–491
56. Sobreira N, Schiettecatte F, Valle D, Hamosh A (2015) GeneMatcher: a matching tool for connecting investigators with an interest in the same gene. Hum Mutat 36:928–930
57. Yan K, Rousseau J, Littlejohn RO, Kiss C, Lehman A, Rosenfeld JR, Stumpel CTR, Stegmann AP, Robak L, Scaglia F, Nguyen TT, Fu H, Ajeawung NF, Camurri MV, Li L, Gardham A, Panis B, Almannai M, Sacoto MJ, Baskin B, Ruivenkamp C, Study D, Study C, Cho MT, Potjer T, Santen GW, Parker MJ, Canham N, McKinnon M, Potocki L, MacKenzie J, Roeder ER, Campeau PM, Yang XJ (2017) Mutations in the chromatin regulator gene BRPF1 causes syndromic intellectual disability and deficient histone acetylation. Am J Hum Genet 100:91–104
58. You L, Yan K, Zou J, Zhao H, Bertos NR, Park M, Wang E, Yang XJ (2015) The lysine acetyltransferase activator Brpf1 governs dentate gyrus development through neural stem cells and progenitors. PLoS Genet 11:e1005034
59. You L, Zou J, Zhao H, Bertos NR, Park M, Wang E, Yang XJ (2015) Deficiency of the chromatin regulator Brpf1 causes abnormal brain development. J Biol Chem 290:7114–7129
60. Sansregret L, Vadnais C, Livingstone J, Kwiatkowski N, Awan A, Cadieux C, Leduy L, Hallett MT, Nepveu A (2011) Cut homeobox 1 causes chromosomal instability by promoting bipolar division after cytokinesis failure. Proc Natl Acad Sci USA 108:1949–1954
61. Gingras H, Cases O, Krasilnikova M, Berube G, Nepveu A (2005) Biochemical characterization of the mammalian Cux2 protein. Gene 344:273–285
62. You L, Zou J, Zhao H, Bertos NR, Park M, Wang E, Yang XJ (2015) Deficiency of the chromatin regulator BRPF1 causes abnormal brain development. J Biol Chem 290:7114–7129
63. Heinsbroek RPW, Vanhaaren F, Vandepoll NE (1988) Sex-differences in passive-avoidance behavior of rats—sex-dependent susceptibility to shock-induced behavioral depression. Physiol Behav 43:201–206
64. Yan K, You L, Degerny C, Ghorbani M, Liu X, Chen L, Li L, Miao D, Yang XJ (2016) The chromatin regulator BRPF3 preferentially activates the HBO1 acetyltransferase but is dispensable for mouse development and survival. J Biol Chem 291:2647–2663
65. You L, Li L, Yan K, Zou J, Belle J, Nijnik A, Wang E, Yang XJ (2016) BRPF1 is essential for development of fetal hematopoietic stem cells. J Clin Invest 126:3247–3262

Publisher's Note Springer Nature remains neutral with regard to jurisdictional claims in published maps and institutional affiliations.